Certifying Robust Generalization with Diverging Spanned Latent Space

Anonymous authors
Paper under double-blind review

Abstract

Robust generalization (RG), concerning how deep neural networks could perform *over adversarial examples generated from unseen dataset*, has emerged as an active research topic. Albeit its crucial importance, most previous studies lack a well-founded theoretical analysis and certified error bounds. In this paper, we make a novel attempt to theoretically and empirically study how we could attain a better RG by learning discriminative representation, where the inconsistency of the inter-sample similarity matrix between clean and adversarial examples should be reduced. Our theoretical investigation discloses that introducing this inconsistency as a regularization term, named Gram matrix difference (GMD), will lead to tighter upper error bound and certify a better RG. Meanwhile, we demonstrate that previous efforts to reduce inter-class similarity and increase intra-class similarity among adversarial examples for enhanced adversarial robustness are approximate optimizations of our GMD approach. Furthermore, to avoid the vast optimization complexity introduced by the similarity matrix, we propose to optimize GMD by building a diverging spanned latent space for adversarial examples. On the algorithmic side, this regularization term is implemented as a novel adversarial training (AT) method — *Subspace Diverging* (SD) — to expand the volume difference between the whole latent space's linear span and subspaces' linear spans. Extensive experiments show that the proposed method can improve advanced AT methods and work remarkably well in various datasets including CIFAR-10, CIFAR-100, SVHN, and Tiny-ImageNet.

1 Introduction

Deep Neural Networks (DNNs) have attained great success recently in various applications, such as image classification, image generation, and object detection. Despite the impressive performance enhancement over various tasks, DNNs are strikingly vulnerable to specific well-crafted adversarial perturbations (Carlini & Wagner, 2017; Song et al., 2018; Fischer et al., 2017; Lyu et al., 2015). Although these perturbations are invisible to humans, they can easily mislead DNNs' predictions. Adversarial training (AT) (Mkadry et al., 2017; Wang & Zhang, 2019; Kannan et al., 2018; Gu & Rigazio, 2015; Zhang & Wang, 2019; Jia et al., 2022) is considered as one of the most effective defense methods capable of effectively improving model robustness against various types of adversarial attacks (Carlini & Wagner, 2017; Croce & Hein, 2020; Kurakin et al., 2016; Mkadry et al., 2017), such as widely used projected gradient descent (PGD) based AT (Mkadry et al., 2017), adversarial weight perturbation (AWP) (Wu et al., 2020), Feature Scatter (FS) (Zhang & Wang, 2019) and TRADES (Zhang et al., 2019).

Although robustness has been improved significantly in previous studies, the robust models trained by most existing adversarial training methods still present poor robust generalization (RG). RG evaluates how well the model trained over the adversarial training set generalizes to further adversarial examples generated from unseen dataset (Rice et al., 2020), which is usually measured by the robust accuracy gap, i.e. the accuracy difference between adversarial training examples and adversarial test examples (Gao et al., 2022). As depicted in Figure 1, all robust AT models, including PGD-AT, AWP, TRADES, and FS show poor RG and present large robust accuracy gaps.

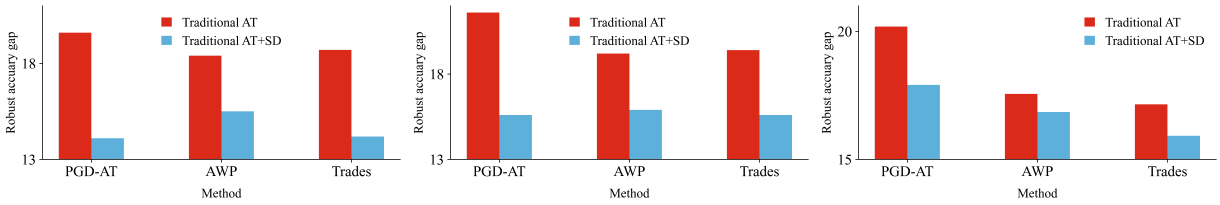

(a) CIFAR-10 (b) CIFAR-100 (c) Tiny-ImageNet

Figure 1: Robust accuracy gap (over PGD20 generated on CIFAR-10, CIFAR-100, and Tiny-ImageNet) between adversarial training and test datasets for classical AT methods and those augmented with our Subspace Diverging (SD) regularization method.

Indeed, RG has been shown even more difficult to achieve than standard generalization, since the sample complexity of adversarial examples can be significantly larger than that of standard or natural samples (Schmidt et al., 2018b). Recent efforts have studied RG from different perspectives, such as introducing customized early stopping (Rice et al., 2020), activation function (Singla et al., 2021), adversarial vertex mixup (Stutz et al., 2021), and diffusion term of Stochastic Differential Equation in AT (Sun et al., 2023). However, most of these methods empirically investigate RG and lack a well-founded theoretical analysis. Recently, Zhang et al. (2021) proposed shift consistency regularization (SCR) term to theoretically certify the RG error, which is, however, shown to be underperformed than our method in experimental results.

In this paper, from the perspective of learning robust and discriminative representation, we aim to investigate an effective algorithm that can certify a tight RG bound in theory, to ensure excellent adversarial robustness practically. Generally, adversarial perturbations induce feature shifts in the latent feature representation (Zhang et al., 2021), which causes adversarial examples to move into the semantic clusters of other classes, resulting in an incorrect classification. This phenomenon can be visualized in Figure 2 by comparing the inter-sample relationship map of clean data with that of adversarial examples. In a standard model, the discriminative features of clean data are similar within the same class and dissimilar among different classes (see Figure 2a). On the contrary, in Figure 2b, features of adversarial examples exhibit smaller intra-class similarity, yet more considerable inter-class similarity than clean data. Ideally, enabling the features of adversarial examples to be as discriminative as clean data will encourage a better RG. Intuitively, this goal can be attained by reducing the inconsistency of inter-sample relationship maps between clean data and adversarial examples.

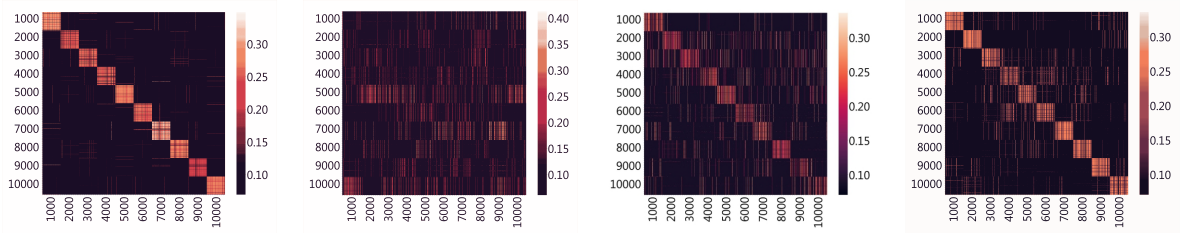

(a) Clean data w/ Sta. (b) PGD20 w/ Sta. (c) PGD20 w/ FS (d) PGD20 w/ FS+SD

Figure 2: Visualization of inter-sample relationship (Gram matrix) of latent features on SVHN. We randomly select 1,000 samples for each class from the test dataset and sort all the selected samples according to their class indexes. The lighter color represents the higher cosine similarity of the two feature vectors, and vice versa. The latent features of a standard model (abbreviated to Sta.) are generated from (a) clean data and (b) adversarial examples perturbed by PGD20. The latent features of adversarial examples perturbed by PGD20 are produced by robust models trained by (c) Feature Scattering (FS) (Zhang & Wang, 2019) and (d) FS applied with our Subspace Diverging (SD). All models are trained on the SVHN dataset and employ wide residual networks (WRN-28) as the backbone.

To further verify our observation, we theoretically analyze the robust generation issue from a novel perspective. We illustrate that the robust generalization gap can indeed be upper bounded by the above inconsistency

of inter-sample relationship - Gram matrix difference. Meanwhile, we demonstrate that previous efforts to reduce inter-class similarity and increase intra-class similarity among adversarial examples for enhanced adversarial robustness in (Li et al., 2019; Bui et al., 2020) are approximate optimizations of our approach. In our case, this term is optimized by learning a diverging spanned latent space for adversarial examples, where **V**olume **D**ifference between the **W**hole latent space's linear span and **S**ubspaces' linear spans (VDWS) is enlarged, such that latent subspaces (divided by categories) to be mutually orthogonal. Our method additionally improves the representation diversity of adversarial examples which has been proved as one of the merits of improving the generalization ability of standard model (Liu et al., 2018). Compared with previous studies like (Li et al., 2019; Bui et al., 2020), our method offers a theoretical guarantee for improving RG through learning discriminative representation. More importantly, compared with (Zhang et al., 2021), our approach enjoys a better RG performance, which can be observed in an empirical analysis in Section 6.5.2, thus certifying robust performance in many real-world datasets.

Built upon the above theory, towards better RG, we instantiate the VDWS with an AT method called *Subspace Diverging* (SD). As shown in Figure 2d, our SD improves the feature representation compared to traditional AT methods (e.g., FS in Figure 2c), which becomes more discriminative and diverse, thus promoting a better RG (as seen in Figure 1). Our contributions are digested as follows:

1) We study and reveal that the robust generalization gap correlates with the difference in inter-sample relationship maps between clean data and adversarial examples. Leveraging this insight, we derive a novel and tighter robust generalization bound.

2) To enable a tractable optimization, we propose to build a diverging spanned latent space for adversarial examples, which is theoretically well-founded for learning discriminate and diverse representation. We implement a novel adversarial regularization method named subspace diverging to achieve this goal.

3) Extensive experiments have been conducted to verify the effectiveness of our adversarial regularization method on various benchmark datasets. The results demonstrate that our approach enhances the performances of various state-of-the-art methods.

2 Related Work

2.1 Adversarial Training

Adversarial training (AT), a primary defense approach against adversarial examples (Goodfellow et al., 2015; Carlini & Wagner, 2017; Athalye et al., 2018), has been extensively researched to enhance the robustness of deep neural networks. Projected gradient descent (PGD) (Carlini & Wagner, 2017) based AT is one most common approach used to enhance robustness, and PGD is an iterative optimization technique designed to generate adversarial examples by perturbing input samples within a specified norm constraint. Adversarial weight perturbation (AWP) (Wu et al., 2020) is proposed which is effective in boosting robustness by directly perturbing the model's weights rather than the input samples. This approach aims to make the model resilient to changes in its model parameters, thereby improving its overall stability and performance against adversarial attacks. Based on AWP, Jin et al. (2023) introduces small Gaussian noise into the weights of the neural network during adversarial training, and the weight perturbation is modeled using a Taylor series expansion, which allows the method to decompose the objective function into multiple terms. The goal is to balance the trade-off between adversarial robustness and clean accuracy by smoothing the weight updates and finding flatter minima in the loss landscape. Feature Scatter (FS) (Zhang & Wang, 2019) disperses features of input data to generate diverse adversarial examples. By ensuring the adversarial examples cover a wider range of perturbations, FS can achieve better robustness. Geometry-Aware Instance Reweighted Adversarial Training (GAIRAT) (Zhang et al., 2020c) optimizes the geometry of decision boundaries by assigning different weights to adversarial examples based on their distances from the decision boundary. GAIRAT effectively balances the trade-off between robustness and accuracy, leading to significant improvements in both areas. Moreover, some researchers also investigate the effects of adversarial training strategies on model performance (Zhang et al., 2020a; Jia et al., 2022; Wei et al., 2023). Friendly Adversarial Training (FAT) (Zhang et al., 2020a) emphasizes that AT from adversarial examples closer to the decision boundary can help in reducing the model's overfitting to adversarial perturbations. Learning attack strategy (LAS) (Jia et al., 2022) is

introduced to adjust attacking configurations for different data samples, and Wei et al. (2023) adapts class-specific training configurations.

2.2 Robust Generalization

Robust generalization evaluates a model's performance against unseen adversarial examples, akin to standard generalization. Yin et al. (2019.) investigate the relationship between model complexity and its ability to robust generalization against adversarial examples. It explores how increasing model capacity can improve adversarial robustness but may also lead to overfitting if not properly regularized. The finding provides theoretical insights and empirical evidence on how to balance model complexity to achieve optimal adversarial robustness and generalization. Schmidt et al. (2018b) argue that achieving robust generalization against adversarial examples necessitates significantly larger datasets compared to standard training. The statement highlights that increased data volume can enhance the model's ability to generalize and resist adversarial attacks. Zhang et al. (2019) decomposes the robust error into natural classification and boundary errors, offering a balanced approach to robustness and accuracy. This study examines the inherent trade-off between achieving robustness against adversarial attacks and maintaining high accuracy on clean data. Li et al. (2022a) analyze that the poor robust generalization is due to the VC dimension of adversarial testing samples being significantly larger than their intrinsic dimension. Sun et al. (2023) enhance robust generalization by approximating PGD-AT as a continuous-time Stochastic Differential Equation (SDE) and manipulating its diffusion term. In (Zhang et al., 2021), the Shift Consistency Regulation (SCR) method is proposed to mitigate deficient robust generalization by reducing variance in perturbation direction between adversarial training and unseen datasets. In this paper, we investigate cosine similarity variants and analyze the robust generalization gap to enhance model robustness. Theoretical analysis suggests that achieving robust generalization faces challenges from random inter-sample relationship variation, susceptible to perturbation attacks. Our approach demonstrates better performance empirically, as observed in our experiments.

2.3 Learning Discriminative and Diverse Representations

Metric learning-based approaches (Cheng et al., 2016b; Hadsell et al., 2006; Hu et al., 2014; Schroff et al., 2015; Huang et al., 2010; Chopra et al., 2005) are employed to increase inter-class distance and decrease intra-class distance for deep features, typically using Euclidean distance. Hadsell et al. (2006) propose how to reduce data dimensionality through invariant feature learning. It focuses on identifying and preserving essential data characteristics while minimizing irrelevant variations, thereby enhancing the efficiency and accuracy of subsequent analyses. The groundbreaking contrastive loss (Hadsell et al., 2006) enforce the above constraints using a siamese network architecture (Chopra et al., 2005). This strategy gained popularity in various downstream tasks such as image retrieval (Yousefzadeh et al., 2023). Moreover, learning discriminative feature representations can also be beneficial in face recognition (Hadsell et al., 2006; Sun et al., 2014), where the triplet loss (Cheng et al., 2016a) and center loss (Wen et al., 2016) also demonstrate similar effectiveness. In a recent work by Lezama et al. (2018), a plug-and-play loss term for deep networks has been utilized to explicitly reduce intra-class variance and enforce inter-class margin. Furthermore, Yu et al. (2020) enhanced feature representation discriminability by augmenting the code rating of feature representation. Following (Yu et al., 2020), Chan et al. (2022) introduce ReduNet, a deep learning framework that constructs interpretable network architectures by maximizing the rate reduction of feature representation. ReduNet efficiently reduces information redundancy and captures essential features.

3 Theoretical Analysis

This section analyzes RG from the theoretical aspect. A novel method is proposed to optimize the robust generalization gap by introducing inter-class and intra-class similarity. Moreover, we propose to leverage volume variety between the whole linear and subspace spans for a tractable optimization, which further improves the diversity of feature representation.

3.1 Robust Representation

Given a data distribution $(x, y) \sim (\boldsymbol{X}, \boldsymbol{Y})$ with K classes, a training set, consisting of N i.i.d. data pairs drawn from $(\boldsymbol{X}, \boldsymbol{Y})$, can be denoted as $(\boldsymbol{X}_D, \boldsymbol{Y}_D)$, where $\boldsymbol{X}_D \in \mathbb{R}^{d\times N}$ and $\boldsymbol{Y}_D \in \mathbb{R}^{K\times N}$ denote a training data matrix and label matrix respectively, and d is the dimension of the data sample. The object of standard generalization is to learn a deep neural network (DNN) $f_\theta(\cdot)$ with parameters θ on a training set so that the generalization error (the difference between the expected loss over data distribution and the empirical loss over the training data) becomes as small as possible (Xu & Mannor, 2012; Bousquet & Elisseeff, 2002; Neyshabur et al., 2017), where $f_\theta(\cdot)$ maps the data samples from input space to latent feature space with dimension r, e.g. $f_\theta(x) \in \mathbb{R}^r$. Leveraging the above insight, considering the loss function $l(\cdot)$ of $f_\theta(\cdot)$, the robust generalization error (gap) (Zhang et al., 2021) is defined as the difference between the expected loss over on adversarial examples $(\boldsymbol{X}_D^{adv}, \boldsymbol{Y}_D)$ and the expected loss over their underlying distribution $(\boldsymbol{X}^{adv}, \boldsymbol{Y})$, i.e.,

$$\varepsilon_{RGE} \triangleq \left| l\left(\boldsymbol{X}^{adv}, \boldsymbol{Y}\right) - l\left(\boldsymbol{X}_D^{adv}, \boldsymbol{Y}_D\right)\right|, \text{where}$$

$$l\left(\boldsymbol{X}^{adv}, \boldsymbol{Y}\right) = \mathbb{E}\left[l\left(f_\theta\left(x^{adv}\right), y\right)\right],$$
$$l\left(\boldsymbol{X}_D^{adv}, \boldsymbol{Y}_D\right) = \frac{1}{N}\sum_{n=1}^{N} l\left(f_\theta(x_n^{adv}), y_n\right).$$

In general, a test set $(\boldsymbol{X}_T, \boldsymbol{Y}_T)$ is introduced as a surrogate of data distribution $(\boldsymbol{X}, \boldsymbol{Y})$ to empirically estimate the robust generalization error since the entire $(\boldsymbol{X}, \boldsymbol{Y})$ is unavailable. Here, $(\boldsymbol{X}_T, \boldsymbol{Y}_T)$ includes i.i.d. samples that are drawn from $(\boldsymbol{X}, \boldsymbol{Y})$ and disjoint with $(\boldsymbol{X}_D, \boldsymbol{Y}_D)$.

In the following, we propose Theorem 3.1 to serve as the main theoretical foundation for our work, which establishes an upper bound of the robust generalization containing standard generalization error and one novel regularization term. This term was inspired based on our observations as illustrated in Figure 2, where the Gram matrix is widely used to measure inter-class and intra-class similarity to capture inter-sample relationships. Detailed proof can be seen in the Appendix.

Theorem 3.1 *Given the clean data matrix $\boldsymbol{X}_i$ and adversarial data matrix $\boldsymbol{X}_i^{adv}$ that both contain N_i samples of i-th class over the training set, the sets of clean data C_i and adversarial data C_i^{adv} of i-th class over the underlying data distribution, and the DNN f_θ that maps data samples to latent features with dimension r, if the loss function $l(\cdot)$ of $f_\theta(\cdot)$ is t Lipschitz and constant values L_d and L_u exist, then for any $\delta > 0$, with the probability at least $1-\delta$, we have*

$$\varepsilon_{RGE} \leq \varepsilon_{GE} + \frac{tU^2L_d}{N}||\nabla \boldsymbol{T}_d||_2 + \frac{tV^2L_u}{K}||\nabla \boldsymbol{T}||_2 + \sqrt{\frac{2K\ln 2 + 2\ln\left(\frac{1}{\sigma}\right)}{N}},$$
$$\text{where} \quad \nabla \boldsymbol{T}_d = \boldsymbol{T}_d^{adv} - \boldsymbol{T}_d, \qquad \nabla \boldsymbol{T} = \boldsymbol{T}^{adv} - \boldsymbol{T},$$
$$U = \frac{1}{N}\sum_{n=1}^{N}||f_\theta(x_n)||_2, \quad V = \frac{1}{K}\sum_{i=1}^{K}||\mathbb{E}\left[f_\theta(x) \mid x \in C_i\right]||_2,$$

M is the upper bound of the loss over the whole underlying data manifold. $\bigtriangledown \boldsymbol{T}_d$ and $\bigtriangledown \boldsymbol{T}$ denote the Gram matrix difference over the training set and the underlying data distribution respectively,

$$\bigtriangledown \boldsymbol{T}_d = \begin{bmatrix} \left(\boldsymbol{Z}_1^{adv}\right)^\top \boldsymbol{Z}_1^{adv} - \left(\boldsymbol{Z}_1\right)^\top \boldsymbol{Z}_1, & \cdots, & \left(\boldsymbol{Z}_1^{adv}\right)^\top \boldsymbol{Z}_K^{adv} - \left(\boldsymbol{Z}_1\right)^\top \boldsymbol{Z}_K \\ \ddots & \ddots & \ddots \\ \left(\boldsymbol{Z}_K^{adv}\right)^\top \boldsymbol{Z}_1^{adv} - \left(\boldsymbol{Z}_K\right)^\top \boldsymbol{Z}_1, & \cdots, & \left(\boldsymbol{Z}_K^{adv}\right)^\top \boldsymbol{Z}_K^{adv} - \left(\boldsymbol{Z}_K\right)^\top \boldsymbol{Z}_K \end{bmatrix},$$
$$\bigtriangledown \boldsymbol{T} = \begin{bmatrix} \left(z_1^{adv}\right)^\top z_1^{adv} - \left(z_1\right)^\top z_1, & \cdots, & \left(z_1^{adv}\right)^\top z_K^{adv} - \left(z_1\right)^\top z_K \\ \ddots & \ddots & \ddots \\ \left(z_K^{adv}\right)^\top z_1^{adv} - \left(z_K\right)^\top z_1, & \cdots, & \left(z_K^{adv}\right)^\top z_K^{adv} - \left(z_K\right)^\top z_K \end{bmatrix}, \tag{1}$$

$$\textit{where} \quad \boldsymbol{Z}_i = \frac{f_\theta\left(\boldsymbol{X}_i\right)}{\|f_\theta\left(\boldsymbol{X}_i\right)\|_{2,col}}, \quad \boldsymbol{Z}_i^{adv} = \frac{f_\theta\left(\boldsymbol{X}_i^{adv}\right)}{\|f_\theta\left(\boldsymbol{X}_i^{adv}\right)\|_{2,col}}, \quad \boldsymbol{Z}_i, \boldsymbol{Z}_i^{adv} \in \mathbb{R}^{r \times N_i},$$
$$z_i = \frac{\mathbb{E}\left[f_\theta\left(x\right) \mid x \in C_i\right]}{\|\mathbb{E}\left[f_\theta\left(x\right) \mid x \in C_i\right]\|_2}, \quad z_i^{adv} = \frac{\mathbb{E}\left[f_\theta\left(x^{adv}\right) \mid x^{adv} \in C_i^{adv}\right]}{\|\mathbb{E}\left[f_\theta\left(x^{adv}\right) \mid x \in C_i^{adv}\right]\|_2}, \quad z_i, z_i^{adv} \in \mathbb{R}^r,$$

$\|\cdot\|_{2,col}$ *represents the calculation of the Euclidean norm of column vectors in the matrix.*

Theorem 3.1 highlights that robust generalization gap ε_{REG} can be decomposed into three terms: 1) the standard generalization gap (ε_{GE}); 2) *Gram matrix difference* (GMD), i.e. $\frac{tU^2L_d}{N}||\nabla \boldsymbol{T}_d||_2 + \frac{tV^2L_u}{K}||\nabla \boldsymbol{T}||_2$, which measures the inter-sample relationship difference between underlying and training adversarial data distribution; 3) a constant component. In GMD, $\bigtriangledown \boldsymbol{T}$ and $\bigtriangledown \boldsymbol{T}_d$ denote the Gram matrix differences on underlying and training data distributions respectively, and both of them aim to quantify the inconsistency of inter-sample relationship maps between clean and adversarial examples. To empirically illustrate the large GMD values of the vanilla AT method, we visualize the Gram matrices on a test set that is randomly sampled and includes $1,000$ data points. Figure 2a and 2c show a $\boldsymbol{T} = \left[\left(\boldsymbol{Z}_i\right)^\top \boldsymbol{Z}_j\right]$ of a standard model and a $\boldsymbol{T}^{adv} = \left[\left(\boldsymbol{Z}_i^{adv}\right)^\top \boldsymbol{Z}_j^{adv}\right]$ of a robust model trained by FS, where $i, j \in \{1, 2, \ldots, K\}$. As observed, the features of adversarial examples present smaller intra-class similarity and larger inter-class similarity than those of clean data, i.e., $||(\boldsymbol{Z}_i^{adv})^\top \boldsymbol{Z}_i^{adv}||_2 < ||\boldsymbol{Z}_i^\top \boldsymbol{Z}_i||_2$ and $||(\boldsymbol{Z}_i^{adv})^\top \boldsymbol{Z}_j^{adv}||_2 > ||\boldsymbol{Z}_i^T \boldsymbol{Z}_j||_2$. This phenomenon results in a value of Gram matrix difference, $\nabla \boldsymbol{T} = \boldsymbol{T}^{adv} - \boldsymbol{T}$, so that a better RG is hard to achieve. Accordingly, we propose to minimize the GMD to reduce this inconsistency and certify a lower RG error.

Comparison to Shift Consistency Regularization (SCR) (Zhang et al., 2021). According to Zhang et al. (2021), for the theoretical analysis of RG, the robust error gap is divided into three components: the standard error gap (ε_{GE}), a constant term, and a feature shift inconsistency term. Therefore, Zhang et al. (2021) propose SCR which constraints the feature shift to certify RG, and SCR $= \min_\theta \frac{t}{N} \sum_{i=1}^K \sum_{v \in \hat{N}_i} \|f_\theta(x_v^{adv}) - f_\theta(x_v) - \mathbb{E}\left[f_\theta(x^{adv}) - f_\theta(x) \mid x \in C_i\right]\|_2^2$, where $\hat{N}_i$ is the set of index of training data for class i. SCR only constrains the difference between the feature shift $f_\theta(x_v^{adv}) - f_\theta(x_v)$ of each training data point and the expectation of feature shifts within the same class for the underlying distribution. Nevertheless, it overlooks the inconsistency among different classes, which intuitively leads to a less tight RG compared to optimizing our GMD. We use an approximated approach to optimizing GMD which is proposed in Section 5, and our method can achieve better RG as empirically shown in Section 6.5.2.

In terms of the optimization of GMD, we can opt to minimize $||\nabla \boldsymbol{T}_d||_2$; however, estimating $||\nabla \boldsymbol{T}||_2$ is generally impractical due to the inaccessibility of the entire underlying distribution. Alternatively, a widely accepted assumption is that the inter-feature relationships within the training data can reflect the structural information of the whole data distribution. This assumption has been effectively utilized in adversarial robustness (Li et al., 2019) and representation learning (Bui et al., 2020). Therefore, as the training feature representations become more discriminative, exhibiting larger intra-class similarity and smaller inter-class similarity, the feature representations of the entire underlying distribution will follow the same trend. Moreover, by learning the discriminative features of adversarial examples, the diagonal elements of the Gram matrix increase, while the off-diagonal elements decrease accordingly for both training and underlying datasets. As such, ignoring the ignoring $||\nabla \boldsymbol{T}||_2$ still represents a reasonable optimization strategy, since the minimizing $||\nabla \boldsymbol{T}_d||_2$ will lead to a decrease in $||\nabla \boldsymbol{T}||_2$.

To address this aspect, we present $||\nabla \boldsymbol{T}_d||_2$ and $||\nabla \boldsymbol{T}||_2$ of our SD, as shown in Figure 3. We empirically calculate these values by randomly sampling $N = 1000$ data points from the training and test set of the CIFAR-10 dataset respectively, where our method is only applied to the training data. $\frac{1}{N^2}||\nabla \boldsymbol{T}_d||_2$ and $\frac{1}{N^2}||\nabla \boldsymbol{T}||_2$ are calculated under the PGD20 and C&W attack with PGD-AT baseline in Figure 3a and 3b respectively. The results clearly illustrate that SD can decrease $||\nabla \boldsymbol{T}_d||_2$ and $||\nabla \boldsymbol{T}||_2$ consistently.

Moreover, GMD can be approximately optimized by minimizing $||\bigtriangledown \boldsymbol{T}_d||_2$, which can be further decomposed as:

$$\|\nabla \boldsymbol{T}_d\|_2 = \sqrt{\|\nabla \boldsymbol{T}_d^{inter}\|_2^2 + \|\nabla \boldsymbol{T}_d^{intra}\|_2^2},$$

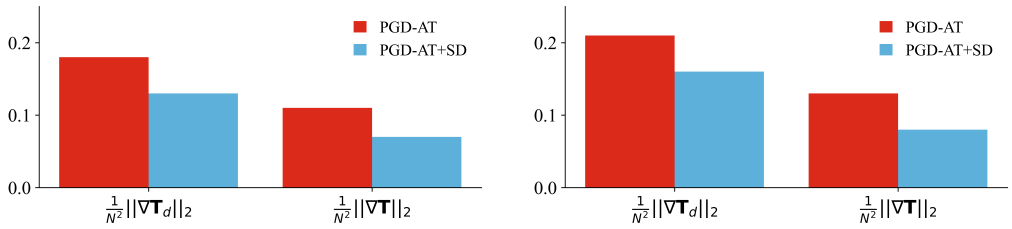

(a) PGD20 (b) C&W

Figure 3: $||\bigtriangledown \boldsymbol{T}_d||_2$ and $||\bigtriangledown \boldsymbol{T}||_2$ of our approach under (a) PGD20 and (b) C&W. All methods are trained by using WiderResNet-34-10 as backbone.

$$\text{where} \quad \|\nabla \boldsymbol{T}_d^{inter}\|_2 = \sqrt{\sum_{i=1}^{K} \sum_{j=1, i\neq j}^{K} \|(\boldsymbol{Z}_i^{adv})^T \boldsymbol{Z}_j^{adv} - (\boldsymbol{Z}_i)^T \boldsymbol{Z}_j\|_2^2}, \tag{2}$$

$$\|\nabla \boldsymbol{T}_d^{intra}\|_2 = \sqrt{\sum_{i=1}^{K} \|(\boldsymbol{Z}_i^{adv})^T \boldsymbol{Z}_i^{adv} - (\boldsymbol{Z}_i)^T \boldsymbol{Z}_i\|_2^2;}.$$

Here, $||\bigtriangledown \boldsymbol{T}_d^{inter}||_2$ and $||\bigtriangledown \boldsymbol{T}_d^{intra}||_2$ denote the inter-class and intra-class similarity respectively on training adversarial example distribution. Reducing $||\bigtriangledown \boldsymbol{T}_d||_2$ can be achieved when $(\boldsymbol{Z}_i^{adv})^\top \boldsymbol{Z}_i^{adv} \longrightarrow \boldsymbol{Z}_i^\top \boldsymbol{Z}_i$ and $(\boldsymbol{Z}_i^{adv})^\top \boldsymbol{Z}_j^{adv} \longrightarrow \boldsymbol{Z}_i^\top \boldsymbol{Z}_j$. Thus, the intra-class cosine similarity should increase, and inter-class cosine similarity should decrease. This solution aligns the general intuition for learning discriminative representation to improve generalization ability and is an approximation of our GMD.

3.2 Diverging Spanned Latent Space

The intricacies of point-to-point level optimization contribute to the vast optimization complexity. To solve this problem, we propose to optimize this term by learning a diverging spanned latent space for adversarial examples.

The linear spans of the whole training feature matrix $\boldsymbol{Z}$ and class-wise feature set $\boldsymbol{Z}_i$ are denoted as $\boldsymbol{S}$ and $\boldsymbol{S_i}$ respectively, and calculated by

$$\boldsymbol{S} = \boldsymbol{Z} \times \boldsymbol{Z}^\top, \boldsymbol{S_i} = \boldsymbol{Z}_i \times \boldsymbol{Z}_i^\top,$$

where $\boldsymbol{S}, \boldsymbol{S}_i \in R^{r\times r}$, r is feature dimension, and column vectors in $\boldsymbol{S}$ and $\boldsymbol{S}_i$ represent the set of basis vectors for the whole latent spaces and class-wise subspace of i-th class. The volume of any latent space linear span $\boldsymbol{P}$ can be represented by its determinant:

$$\text{Vol}\left(\boldsymbol{P}\right) = \det\left(\boldsymbol{P}\right). \tag{3}$$

Intuitively, the more diverse the subspaces are, the more separable clusters of adversarial example feature representation. Consequently, the inter-class similarity tends to decrease. Such a latent space, composed of diverging subspaces, embodies a larger volume, which is visualized in Figure 4. Besides, a smaller volume of each subspace indicates a larger intra-class similarity. We show the proof details of this viewpoint in Theorem 3.2.

Theorem 3.2 *Let the latent space span $\boldsymbol{S}$ be a non-singular matrix that covers all subspans and is denoted as $\{\boldsymbol{S}_i\}_{i=1}^K \in \boldsymbol{S}$, and $\boldsymbol{I}$ be the identity matrix. For any vectors $\gamma_i, \gamma_j \in S_i$, S_j, where $\forall i, j \leq K$, and $i \neq j$, and vectors $\gamma_{iu}, \gamma_{iv} \in \boldsymbol{S}_i$, the implication relationship is:*

$$\begin{aligned} \max \text{Vol}(\boldsymbol{S}) &\Longrightarrow \min \left\langle \gamma_i, \gamma_j \right\rangle, \\ \min \text{Vol}(\boldsymbol{I} + \boldsymbol{S}_i) &\Longrightarrow \max \left\langle \gamma_{iu}, \gamma_{iv} \right\rangle. \end{aligned} \tag{4}$$

Theorem 3.2 highlights that decreased cosine similarity among distinct subspaces basis expands the volume of the overall spanned latent space as illustrated in Figure 4. In contrast, heightened cosine similarity between intra-class basis is associated with reduced volume in each subspace. Detailed proof of Theorem 3.2 is provided in the Appendix.

To achieve a discriminative feature representation, we aim to maximize the overall volume of the training latent space linear span while minimizing the volume of the linear subspace span, as elaborated in Section 3.1. Specifically, we sort these objectives by prioritizing the expansion of the **V**olume **D**ifference between the **W**hole latent space's linear span and **S**ubspaces' linear spans (VDWS):

$$VDWS \triangleq \mathrm{Vol}\left(\boldsymbol{S}^{adv}\right) - \frac{1}{K}\sum_{i=1}^{K}\mathrm{Vol}\left(\boldsymbol{I} + \boldsymbol{S}_i^{adv}\right), \tag{5}$$

where $\boldsymbol{I}$ is the identity matrix to prevent the subspace S_i volume being close to 0; hence, the above issue can be reformulated as aiming to maximize VDWS to diminish concurrently both $||\nabla \boldsymbol{T}_d^{inter}||_2$ and $||\nabla \boldsymbol{T}_d^{intra}||_2$, denoted as:

$$\max VDWS \Longrightarrow \min ||\nabla \boldsymbol{T}_d||_2, \tag{6}$$

where $||\nabla \boldsymbol{T}_d||_2$ represents the gram matrix difference on whole data distribution.

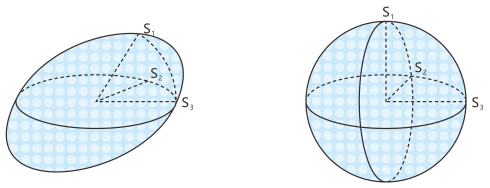

Figure 4: As the subspace becomes more independent, the volume of the overall spanned space becomes larger (each small white ball represents the unit volume, and as the white ball becomes more extensive, the overall volume becomes more prominent). Therefore, semantic clusters may become more dispersed, resulting in more discriminative feature representations.

Here, we show that maximizing VDWS enjoys an additional advantage for certifying better robust generalization since the diversity of adversarial example feature representations is implicitly promoted. Specifically, VDWS that builds a diverging spanned latent space will produce a *unique eigenvector set* for each subspace, including a more significant number of eigenvectors.

By applying the singular value decomposition algorithm, the subspace can be denoted as $\boldsymbol{S}_i = \boldsymbol{U}_i \sum_i \boldsymbol{V}_i^\top$, where $\boldsymbol{U}_i$ represents the eigenvector matrix of $\boldsymbol{S}_i$. The *unique eigenvector set* for i-th class, including the orthogonal basis set that remains independent of other subspaces, is defined as:

$$\begin{aligned} \boldsymbol{U}_i^* &= \{e_{i_1}, ..., e_{i_t}, ..., e_{i_T}\}, \\ \text{s.t.} \quad e_{i_t} \times \boldsymbol{S}_j &= 0, \quad \forall\ e_{i_t} \in \boldsymbol{U}_i^*,\ j \in [1, K] \text{ and } i \neq j. \end{aligned} \tag{7}$$

Since our VDWS increases the volume of $\boldsymbol{S}$, the more significant number of the whole latent space basis will be attained so that the number of bases e_{i_t} in unique eigenvector set $\boldsymbol{U}_i^*$ of subspace also increases.

From the above analysis, a more sizable number of distinct eigenvectors e_{i_t} in $\boldsymbol{U}_{i_{adv}}^*$ will naturally steer to a greater value of $rank(\boldsymbol{U}_{i_{adv}}^*)$, which has been shown as a necessary condition for learning diverse representation in (Chan et al., 2022). Therefore, the approach not only enhances feature representation discrimination but also improves feature representation diversity, which has been proven to enhance model generalization (Liu et al., 2018). Moreover, We further verify the feature diversity of our method through experimental analysis in Section 6.5.1.

Previous studies have investigated the discriminative and diverse representation learning for standard generalization, such as Maximal Coding Rate Reduction (MCR^2), considering the low level of feature distortion as an essential premise in (Yu et al., 2020). However, as shown in Figure 2b and 2c, features of adversarial

examples are highly distorted, which leads to unclear inter-sample relationships. As a result, applying MCR^2 directly on an adversarial example potentially introduces difficulty in the optimization process. In contrast, we propose to work on the volume to maximize VDWS to achieve robust generalization.

4 Empirical Analysis

In this section, we aim to confirm the validity of Theorem 3.1 by demonstrating how the accuracy gap between test and training adversarial examples evolves with varying values of VDWS. We visually illustrate inter-sample similarity, shedding light on how adversarial perturbations play a role in this accuracy gap. All the models discussed in this subsection are trained using Feature Scatter (FS) on the SVHN dataset.

4.1 Robust Generalization vs. Volume of Linear Span

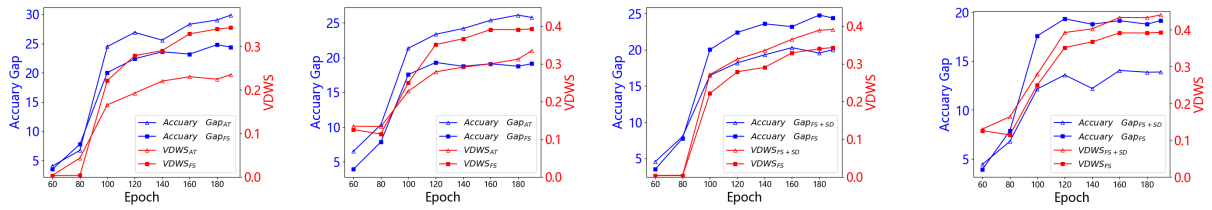

(a) (b) (c) (d)

Figure 5: The accuracy gap vs. VDWS$_t$ at different training epochs. The comparison of FS and AT to train the robust models against various attacks: (a) C&W attack and (b) PGD20 attack. The comparison of FS and FS+SD (ours) to train the robust models against various attacks: (c) C&W attack and (d) PGD20 attack.

Adhering to the established evaluation protocol (Xu & Mannor, 2012), rather than using the error gap difference $|\varepsilon_{RGE} - \varepsilon_{GE}|$, we choose to calculate the accuracy gap difference, $\big||ACC(\boldsymbol{X}_T^{adv}, \boldsymbol{Y}_T) - ACC(\boldsymbol{X}_D^{adv}, \boldsymbol{Y}_D)| - |ACC(\boldsymbol{X}_T, \boldsymbol{Y}_T) - ACC(\boldsymbol{X}_D, \boldsymbol{Y}_D)|\big|$ which shares the same trend with error gap difference. This replacement will provide a direct reflection of robust generalization, which has been widely utilized in previous studies (Zhang et al., 2021). In Section 3.1, we have demonstrated the correlation between VDWS and GMD. To validate Theorem 3.1 and show whether the gap difference is caused by GMD, the VDWS$_t$ and the accuracy gap difference under C&W and PGD20 across 60 to 200 epochs are shown in Figure 5a and 5b, where robust models are trained by FS and AT respectively and VDWS$_t$ denote the VDWS values of the test datasets. As results can be observed, the VDWS$_t$ and the accuracy gap difference show obvious consistency. Therefore, the results indicate that GMD can capture the error gap difference (reflecting the difference between robust and standard generalization).

Feature Visualization

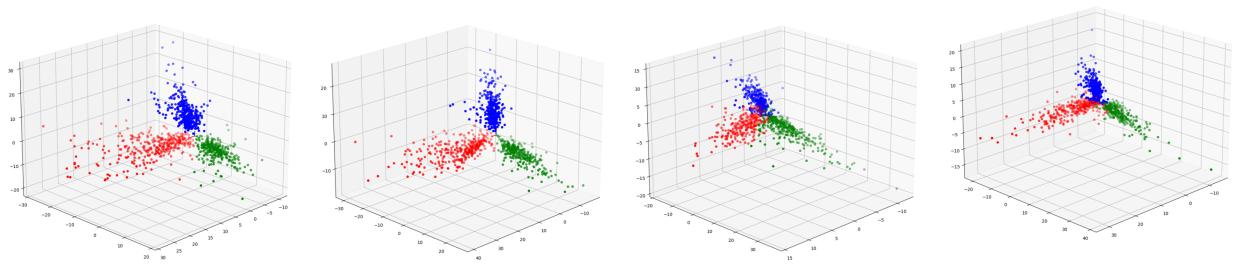

(a) Clean w/ FS (b) Clean w/ FS+SD (c) PGD3 w/ FS (d) PGD3 w/ FS+SD

Figure 6: The latent features generated from (a) FS with clean samples, (b) FS+SD with clean samples, (c) FS against PGD3 attack, (d) FS+SD against PGD3 attack. All models are trained on the CIFAR-10 dataset and employ wide residual networks (WRN-28) as the backbone.

We select three classes for visualizing the feature distributions on the test dataset of CIFAR-10. We employ a multi-layer perceptron (MLP) backbone and utilize a PGD-3 attack with $\epsilon = \frac{2}{255}$ to generate feature distributions presented in Figure 6. In the latent space of adversarial examples, after integrating our SD to FS in Figure 6d, the distributions of the categories are more inclined toward the vertical, and the clusters of categories are more compact than the ones of FS in Figure 6c. This trend also emerges in the clean dataset, as observed in models trained by FS+SD in Figure 6b and FS in Figure 6a.

5 Subspace Diverging Regularization

We now turn to solve the optimization problem outlined in Section 3.2. Initially, to expand the entire volume of the latent linear span $\mathrm{Vol}\,(\boldsymbol{S})$, we introduce the following functions:

$$L_{\text{span}} = \log\det(\boldsymbol{S}). \tag{8}$$

The function $\log\det(\cdot)$ is a smoothly concave function that aids in achieving an optimal solution more effectively. Moving on, to reduce the volume of the subspace linear span, we define the contraction component as below:

$$L_{\text{shrink}} = \sum_{i=1}^{K} \frac{N_i}{2N} \log\det\left(\boldsymbol{I} + \frac{\omega}{N_i}\boldsymbol{S_i}\right), \tag{9}$$

where N_i represents the number of training samples for each class, and ω is a pre-defined parameter. These two components collaboratively function as:

$$L_{\text{diverge}} = \gamma L_{\text{shrink}} - (1-\gamma) L_{\text{span}}, \tag{10}$$

where γ is a balance hyper-parameter, scaling two functions effectively.

Algorithm 1 Adversarial Training with our Subspace Diverging (SD)

Input: a neural network $f_\theta(\cdot)$ initialized with learnable parameters θ, $\hat{n}$ batches of data pairs $\{(\hat{x}_1, \hat{y}_1), (\hat{x}_2, \hat{y}_2), \ldots, (\hat{x}_{\hat{n}}, \hat{y}_{\hat{n}})\}$, batch size V, a predefined hyper-parameter λ, Gaussian noise $\epsilon \in (-0.015, 0.015)$, number of epochs e.
Output: robust neural network $f_\theta(\cdot)$.
Initialize $L_{gene}^{max} \leftarrow 0$, $L_{diverge}^{max} \leftarrow 0$, $L^{max} \leftarrow 0$
for $i \leftarrow 1$ to $\hat{n}$ **do**
  Add Gaussian noise on data samples: $\hat{x}_i' = \hat{x}_i + \epsilon$
  Generate the adversarial examples for i-th data batch: $\hat{x}_i^{\text{adv}} \leftarrow \underset{\hat{x}_i'}{\text{argmax}}\left(L_{\text{gene}}(\hat{x}_i', \hat{y}_i, \theta)\right)$
  Select the maximum loss values for three sets:
    $L_{gene}^{max} \leftarrow \max(L_{gene}(\hat{x}_i', \hat{y}_i, \theta), L_{gene}^{max})$
    $L_{diverge}^{max} \leftarrow \max(L_{diverge}(\hat{x}_i', \hat{y}_i, \theta), L_{gene}^{max})$
    $L^{max} \leftarrow \max(L(\hat{x}_i^{adv}, \hat{y}_i, \theta), L^{max})$
end for
Calculate the k and d by: $k = \frac{L_{diverge}^{max}}{L^{max}}$ and $d = \frac{L_{diverge}^{max}}{L_{gene}^{max}}$
for $j \leftarrow 1$ to e **do**
  for $i \leftarrow 1$ to $\hat{n}$ **do**
    $\hat{x}_i' \leftarrow \hat{x}_i + \epsilon$
    Generate the adversarial examples: $\hat{x}_i^{\text{adv}} \leftarrow \underset{\hat{x}_i'}{\arg\max}\left(L_{\text{gene}}(\hat{x}_i', \hat{y}_i, \theta) + \frac{1}{d} L_{\text{diverge}}(\hat{x}_i', \hat{y}_i, \theta)\right)$
    Update the classifier: $\theta \leftarrow \underset{\theta}{\min}\left\{\frac{1}{V}\left(L(\hat{x}_i^{\text{adv}}, \hat{y}_i, \theta) + \frac{\lambda}{k} L_{\text{diverge}}(\hat{x}_i^{\text{adv}}, \hat{y}_i, \theta)\right)\right\}$
  end for
end for
return robust neural network $f_\theta(\cdot)$.

Table 1: All used hyper-parameters on different methods.

Method	Datasets	Batch Size	Training Epoch	(d,k)	γ	λ	ω
PGD-AT+SD	CIFAR-10	120	400	(100,100)	0.5	0.5	0.05
	CIFAR-100	80	300	(200,200)	0.7	0.05	0.01
	Tiny-ImageNet	120	120	(200,400)	0.2	0.01	0.05
AWP+SD	CIFAR-10	120	200	(100,100)	0.5	0.5	0.1
	CIFAR-100	120	250	(200,200)	0.7	0.02	0.1
	Tiny-ImageNet	120	130	(150,400)	0.3	0.01	0.5
FS+SD	CIFAR-10	120	300	(200,100)	0.5	0.5	0.1
	CIFAR-100	100	400	(200,150)	0.5	0.02	0.05
	SVHN	120	600	(200,100)	1	0.05	0.05
TRADES+SD	CIFAR-10	80	90	(90,50)	0.8	0.1	0.05
	CIFAR-100	100	90	(150,200)	0.5	0.01	0.01

Consequently, we propose utilizing L_{diverge} as a regularization term in adversarial training. This regularization promotes subspace divergence, which can be defined as:

$$\min_{\theta} \{\frac{1}{N} L\left(\boldsymbol{X}_D^{adv}, \boldsymbol{Y}_D, \theta\right) + \frac{\lambda}{k} * L_{\text{diverge}}\ \left(\boldsymbol{X}_D^{adv}, \boldsymbol{Y}_D, \theta\right)\},$$
$$\text{s.t. } \boldsymbol{X}_D^{adv} = \underset{X'_D}{\text{argmax}} \left(L_{gene}\left(\boldsymbol{X}'_D, \boldsymbol{Y}_D, \theta\right) + \frac{1}{d} L_{\text{diverge}}\ \left(\boldsymbol{X}'_D, \boldsymbol{Y}_D, \theta\right) \right),$$

where $\boldsymbol{X}_D^{adv}$ indicate adversarial training dataset that are produced during the adversarial training, $\boldsymbol{X}'_D$ represents the initial adversarial training dataset that adds random noise to the original image, $L(\cdot)$ is an adversarial training loss, and $L_{gene}(\cdot)$ is the loss function which producing adversarial examples. As the scale of $L_{diverge}(\cdot)$ and $L_{gene}(\cdot)$ are different, we design normalization parameters d and k to adjust loss values, and λ is an additional pre-defined parameter.

Due to the GPU memory limitations, calculating $L_{diverge}(\cdot)$ for all of the training dataset is very challenging. To solve this problem, we calculate $L_{diverge}(\cdot)$, $L(\cdot)$, and $L_{gene}(\cdot)$ for each data batch. Then, we select the maximum values among all the batches and define them as L^{max}, L^{max}_{gene}, and $L^{max}_{diverge}$ respectively. Subsequently, we estimate d and k using L^{max}, $L^{max}_{diverge}$ and L^{max}_{gene}, where $d = \frac{L^{max}_{diverge}}{L^{max}_{gene}}$ and $k = \frac{L^{max}_{diverge}}{L^{max}}$.

We have observed that the values of d and k remain stable for each epoch. Therefore, to streamline our training process, we compute the d and k only in the first epoch. The specific values for d and k of various datasets and the entire algorithm can be found in experiment section. When training the generated adversarial examples, our algorithm can be regarded as a regularization to increase the overall spanned space volume but reduce the volume of each subspace.

6 Experiments

This section conducts comprehensive experiments to gauge the effectiveness of our SD method, in countering diverse adversarial examples.

6.1 Experimental Setting

We evaluate our method's robustness against white-box and black-box adversarial examples on CIFAR-10, CIFAR-100, SVHN, and Tiny-Imagenet. We benchmark our approach against four established methods: Feature Scattering (FS) (Zhang & Wang, 2019), Adversarial Training (AT) (Mkadry et al., 2017), Adversarial Weight Perturbation (AWP) (Wu et al., 2020), and TRADES (Zhang et al., 2019). Our core model is based on the WideResNet-34-10 (WRN34) architecture. On Tiny-ImageNet datasets, we follow (Jia et al., 2022) and implement PreActResNet18 as the backbone. FS, a well-known baseline, has been demonstrated to

Table 2: Accuracy under white-box attacks on CIFAR-10 and CIFAR-100 with WiderResNet-34-10.

Method	CIFAR-10					CIFAR-100				
	Clean	PGD-20	PGD-50	C&W	AA	Clean	PGD-20	PGD-50	C&W	AA
PGD-AT	85.17	55.08	54.88	53.91	51.69	60.89	31.69	31.45	30.10	27.86
TRADES	85.72	56.10	55.90	53.87	53.40	58.61	28.66	28.56	27.05	25.94
AWP	85.57	58.13	57.92	56.03	53.90	60.38	33.86	33.65	31.12	28.86
LBGAT	88.22	54.66	54.30	54.29	52.23	60.64	34.75	34.62	30.65	29.33
MART	84.17	58.56	58.06	54.58	51.10	-	-	-	-	-
FAT	87.97	49.86	48.79	48.65	47.48	-	-	-	-	-
GAIRAT	86.30	59.54	58.74	45.57	40.30	-	-	-	-	-
SAT	-	-	-	-	-	62.82	27.17	26.76	27.32	24.57
PGD-AT+LAS	86.23	56.49	56.12	55.73	53.58	61.80	32.77	32.54	31.12	29.03
PGD-AT+SCR	85.91	56.91	56.51	54.93	53.04	60.90	32.97	31.58	30.39	29.17
PGD-AT+RAT	84.39	56.29	55.97	55.18	52.38	61.15	32.29	30.97	31.53	28.77
TRADES+LAS	85.24	57.07	56.80	55.45	54.15	60.62	32.53	32.39	29.51	28.12
TRADES+SCR	86.31	56.81	55.97	54.29	54.10	60.42	32.15	32.17	29.57	27.68
TRADES+RAT	85.98	58.47	-	56.13	54.20	62.93	33.36	-	29.61	27.90
AWP+LAS	87.74	60.16	59.79	58.22	55.52	64.89	36.36	36.13	33.92	30.77
AWP+SCR	85.49	60.90	58.31	56.36	53.49	64.51	34.92	33.98	33.58	29.79
AWP+RAT	86.12	61.45	-	58.22	57.40	64.71	35.73	-	31.41	30.20
PGD-AT+SD	86.43	58.93	58.29	55.79	53.91	62.34	33.19	32.97	31.99	29.58
TRADES+SD	85.99	58.79	57.03	56.93	55.03	60.97	33.79	33.17	29.79	28.43
AWP+SD	**87.79**	**61.59**	**60.30**	**58.73**	**57.91**	**64.91**	**36.59**	**35.97**	**34.03**	**31.14**

perform poorly against strong attacks, such as Autoattack, in previous work (Naseer et al., 2022). As a result, we do not present it as a primary outcome. However, since SCR is built upon FS, we will compare SD with SCR based on FS baseline alone in Section 6.3. Following (Zhang et al., 2021), we implement WideResNet-28-10 (WRN28) for comparison.

In our training regimen, we employ SGD with a momentum of 0.9, weight decay of 5×10^{-4}, and an initial learning rate of 0.1. Learning rates decrease at epochs 60 and 90 by a factor of 0.1. During training, we perform 7 attack iterations for PGD-AT and TRADES, and 1 iteration for FS. For consistency, the attack budget ϵ is maintained at 8/255 for all the methods. Adversarial examples are computed with the ℓ_∞ norm during training and testing. All experiments are conducted on a single GPU, e.g. RTX 3090, under the environment using CUDA 11.7, Python 3.8, and Pytorch 1.80. Table 1 lists all used parameters on different baselines, batch sizes, and training epochs. The γ is the balance parameter, ω and λ are pre-defined parameters, d and k are normalization parameters. The early stopping is used for model selection in all methods.

6.2 Robustness against Adversarial Examples

Our results reveal that SD can improve the robustness of different baselines against attacks on various datasets. Even for more complex datasets such as Tiny-imagine, SD still has a significant effect compared with baselines.

Based on various baselines, we compare our proposed baseline+SD approach with other state-of-the-art adversarial training methods : 1) PGD-AT (Mkadry et al., 2017), 2) AWP (Wu et al., 2020), 3) FS (Zhang & Wang, 2019). 4) SCR (Zhang et al., 2021), 5) LAS(Jia et al., 2022), 6) GAIRAT (Zhang et al., 2020c), 7) SAT (Sitawarin et al., 2021), 8) FAT (Zhang et al., 2020b), and 9) RAT (Jin et al., 2023). We report the results under the white-box attack in Table 2, Table 3, and Table 4 while leaving the results of the black-box attack in Table 6.

Table 2 demonstrates the robust accuracy under various attacks on CIFAR-10 and CIFAR-100. Our method consistently demonstrates better test accuracy across diverse

Table 3: Accuracy under white-box attack on Tiny-Imagenet.

Method	Clean	PGD20	PGD50	C&W	AA
PGD-AT	41.98	20.43	19.98	17.60	13.78
AWP	41.48	22.79	22.51	19.02	17.34
PGD-AT+LAS	44.86	22.29	22.16	18.54	16.74
AWP+LAS	45.26	23.77	23.42	19.88	18.42
PGD-AT+SD	44.27	23.15	22.97	18.59	16.79
AWP+SD	**45.59**	**23.91**	**23.49**	**20.07**	**18.81**

adversarial scenarios, even for clean data, showcasing a notable 2.2% improvement on AWP. On CIFAR-100, our SD also demonstrates superior performance against adversarial examples on various benchmarks such as PGD-AT and AWP. Notably, SD's remarkable effectiveness is particularly evident in C&W with a 2.7% improvement, and in PGD20 with a 3.5% improvement for AWP. Compared to the TRADES method, the TRADES+SD approach demonstrates superior performance across clean samples and various attacks, particularly achieving improvements to 58.79% and 57.03% under PGD-20 and PGD-50 attacks, respectively. Similarly, for AWP, there is a noticeable improvement of 2.9% for CW and 2.7% for PGD20 on CIFAR-100. The TRADES+SD consistently outperforms others in terms of accuracy under clean data and various attacks, notably reaching 33.17% accuracy under the PGD-50 attack. These results underscore the effectiveness and robustness of the SD method. Shifting the focus to Tiny-ImageNet as depicted in Table 3, SD augmentation notably enhances AWP by over 1.5% and PGD-AT by over 3.0% on Autoattack.

Table 4 shows the performance of robust models against white-box attacks on the SVHN dataset. FS+SD demonstrates superior robustness, outperforming all other methods against PGD20, PGD100, and C&W with accuracies of 74.15%, 66.57%, and 65.91%, respectively. These results indicate that SD significantly enhances robustness against other adversarial attacks.

Table 4: Accuracy under white-box attacks on SVHN ($\epsilon = 8$).

Models	Clean	PGD20	PGD100	C&W
Standard	**97.20**	0.30	0.10	0.30
PGD-AT (Mkadry et al., 2017)	93.90	47.90	46.00	48.70
LAT (Kumari et al., 2019)	91.65	60.23	59.97	-
Bilateral (Wang & Zhang, 2019)	94.10	53.90	50.30	-
FS (Zhang & Wang, 2019)	96.20	62.90	52.00	61.30
FS+SCR (Zhang et al., 2021)	96.60	70.24	60.72	64.42
FS+SD	97.10	**74.15**	**66.57**	**65.91**

The effectiveness of SD is validated across different scenarios, from CIFAR-10 to CIFAR-100, SVHN and even to Tiny-ImageNet, as well as against different types of adversarial attacks. This indicates that SD is a reliable method for enhancing the robustness of deep learning models.

6.3 Results on FS baseline compared with SCR

Table 5 presents the performance of different methods based on the FS baseline on CIFAR-10, CIFAR-100 and SVHN. Notably, the results marked with an asterisk (*) are cited from (Naseer et al., 2022). On CIFAR-10, SD performs worse than SCR against certain attacks, such as PGD20. However, on CIFAR-100 and SVHN, SD comprehensively outperforms SCR. These results prove that SD can achieve better robust accuracy compared with SCR.

Table 5: Accuracy under white-box attack on FS baseline with WiderResNet-28-10.

Dataset	Method	Clean	PGD-20	PGD-100	C&W	AA
CIFAR-10	FS	90.00	70.50	68.60	62.40	36.64
	FS+SCR	**92.70**	**76.45**	67.79	**75.42**	35.81
	FS+SD	91.91	72.33	**71.85**	68.66	**37.85**
CIFAR-100	FS	73.90	47.20	46.20	34.60	0.00*
	FS+SCR	74.20	48.87	47.34	38.90	-
	FS+SD	**74.55**	**51.03**	**49.57**	**41.53**	**4.77**
SVHN	FS	96.20	62.90	52.00	61.30	25.26
	FS+SCR	96.60	70.24	60.72	64.62	-
	FS+SD	**97.10**	**74.15**	**66.57**	**65.91**	**33.51**

6.4 Results on Black-Box Attack

Table 6 presents the robust accuracies under black-box attacks on three datasets, including CIFAR-10, CIFAR-100, and Tiny-ImageNet. Here, since the compared methods are evaluated by using different backbones in original papers, it is difficult to compare the results of black-box attacks directly. To ensure a fair comparison, we retrain all compared methods by leveraging the WiderResNet-34-10 (WRN34) as the unified backbone and maintaining their original training parameter. We implement two black-box attacks FAB and SQUARE belonging to Autoattack. For CIFAR-10, the AWP+SD method outperforms others with a large margin on accuracies of 63.02% against FAB attacks and 63.88% against SQUARE attacks. In CIFAR-100, AWP+SD also leads, achieving 31.72% accuracy for FAB and 37.90% for SQUARE, marking it as the most resilient method in this dataset as well. On Tiny-ImageNet, AWP+RAT reports the best performance against FAB attacks with an 18.16% accuracy, while AWP+SD achieves the top score against SQUARE attacks at 24.49%. The results suggest that SD generally provides the best defense for various datasets.

Table 6: Accuracy under transfer-based black-box attack various datasets ($\epsilon = 8$).

Method	CIFAR-10		CIFAR-100		Tiny-ImageNet	
	AA_{FAB}	$\text{AA}_{\text{SQUARE}}$	AA_{FAB}	$\text{AA}_{\text{SQUARE}}$	AA_{FAB}	$\text{AA}_{\text{SQUARE}}$
AWP (Wu et al., 2020)	60.51	61.28	30.97	35.88	17.19	22.91
AWP+LAS (Jia et al., 2022)	62.41	63.39	31.20	37.29	17.82	24.42
AWP+RAT (Jin et al., 2023)	61.75	63.25	30.09	36.10	**18.16**	22.98
AWP+SCR (Zhang et al., 2021)	62.01	62.29	31.10	35.49	17.52	23.61
AWP+SD	**63.02**	**63.88**	**31.72**	**37.90**	17.73	**24.49**

6.5 Further Analysis

We now examine the relationship between the accuracy gap and VDWS to illustrate the effectiveness of SD. In addition, we utilize feature vector maps to manifest the SD performance.

6.5.1 Generalization Analysis

Figures 5c and 5d illustrate the robust accuracy gap under C&W and PGD20 between training and test datasets of CIFAR-10. We present VDWS_t for both the FS and FS+SD. Notably, Figures 5c and 5d highlight that FS+SD achieves a smaller accuracy gap and a greater VDWS_t in comparison to FS. FS+SD consistently maintains superior VDWS_t throughout the convergence process and exhibits a reduced accuracy gap. This observation underscores SD's role in diminishing the accuracy gap and enhancing robust generalization by emphasizing the volume difference between the entire space and the summation of subspaces.

6.5.2 Comparison of RG with SCR

Figures 7a and 7b illustrate a comparison of RG results obtained through optimization using the SD regularization term versus the SCR regularization term. We use PGD-AT as a baseline and attacks are PGD20 and C&W, respectively. It is evident that using the SD regularization term results in a smaller RG compared to the SCR regularization term. The reason is that compared to SCR, SD not only constrains the inter-sample relationship variations within the same class but also increases the inter-class similarity. The outcomes validate that SD can achieve better RG compared with SCR term.

6.5.3 Diversity Analysis

According to the definition given in Equation 7, an increase in the total unique vector numbers reflects greater feature representation diversity. However, the computation of unique eigenvector numbers poses a challenging task. To facilitate direct measurement of the diversity within the spanned space $\boldsymbol{S}$, we utilize a widely adopted evaluation metric, effective rank, denoted as $Erank$. It can be mathematically represented

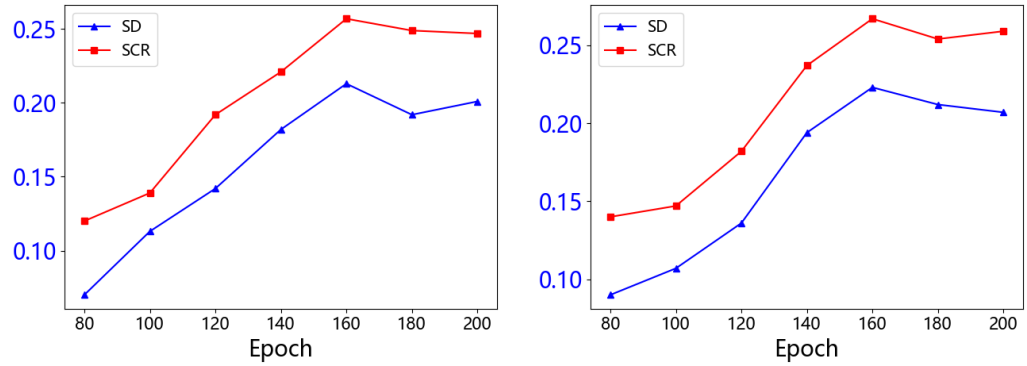

(a) PGD20 (b) C&W

Figure 7: RG with PGD-AT+SD and PGD-AT+SCR on CIFAR-100 under (a) PGD20 and (b) C&W. All methods are trained by using WiderResNet-34-10 as backbone.

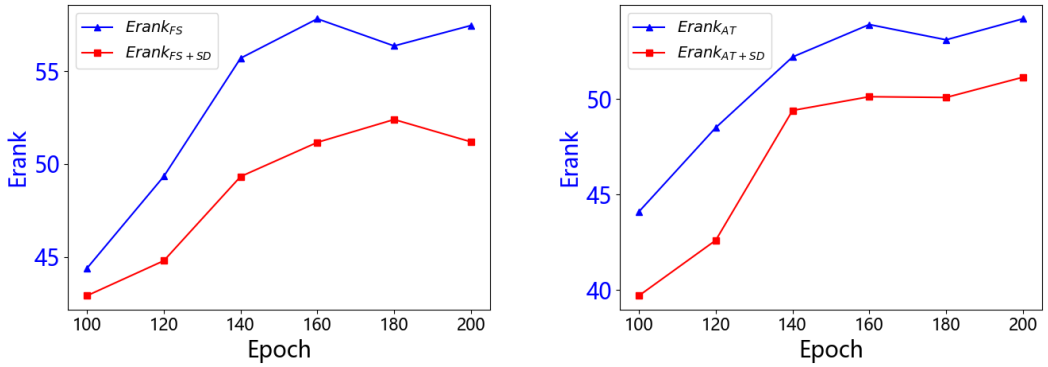

(a) FS baseline (b) AT baseline

Figure 8: *Erank* values under PGD20 attacks from the CIFAR-100 dataset.

as:

$$Erank(\boldsymbol{S}) = exp\left(-\sum_{l=1}^{L} p_l log\left(p_t\right)\right), \quad p_l = \frac{\alpha_l}{||\alpha||_1}, \tag{11}$$

where α_l denote the l-th element in an eigenvalue set $\alpha = \{\alpha_1, \ldots, \alpha_l, \ldots, \alpha_L\}$ of the spanned space $\boldsymbol{S}$, $||\alpha||_1$ represents the L1 norm of α, and p_l is the normalized eigenvalue. The larger *Erank* represents the better diversity for feature representation. When the values of *Erank* reach maximum, the determinant of $\boldsymbol{S}$ (i.e. $\det(\boldsymbol{S}) = \prod_{l=1}^{L} \alpha_l$) also reach maximum. Following the above analysis, we can conclude that there is a positive relationship between VDWS and *Erank*. Increasing the VDWS corresponds to an enlargement of *Erank*. Meanwhile, Figure 8 also validates this statement. Figures 8a and 8b illustrate that SD enhances *Erank* values of both FS and AT under PGD20 attacks to enhance feature diversity.

6.5.4 Sensitivity Analysis

We examine the parameter sensitivity of γ and λ on CIFAR-10 in Figure 9. In Figure 9a, we can observe that the effect of the *shirnk* term is greater than that of the *expand* term since the ratio of the *expand* term is $(1-\gamma)$. Figure 9b shows that our method is less sensitive to λ as the fluctuation is only around 2.5%.

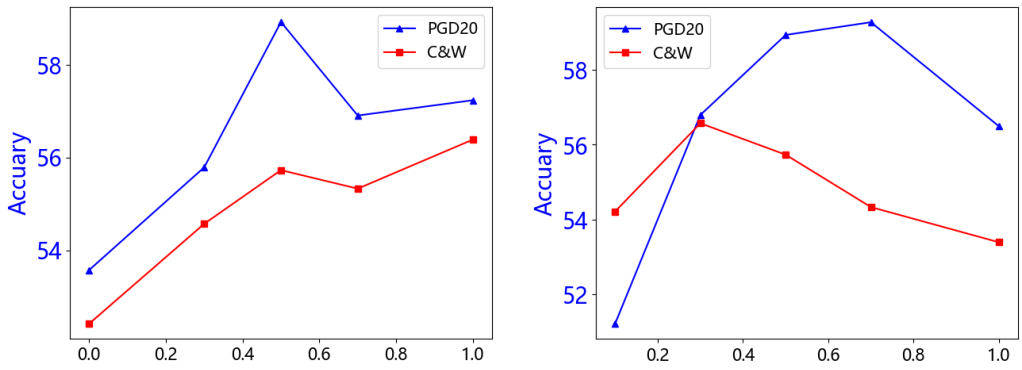

(a) γ (b) λ

Figure 9: Parameter sensitivity for γ and λ on CIFAR-10, where all models are trained by AT+SD.

Conclusion

In this paper, we investigate the robust generalization (RG) problem from the perspective of learning discriminative representation for adversarial examples. Our theoretical and empirical analysis illustrate that reducing the inconsistency of inter-sample relationship maps between clean data and adversarial examples is a feasible approach to alleviate robust overfitting and can be calculated by the proposed Gram matrix difference (GMD). Meanwhile, we provide a theoretical guarantee for RG by introducing a novel and tight error bound based on our GMD. Moreover, to ease the complex optimization of inter-sample relationship maps, we propose a method that expands the volume difference between the entire latent space's linear span and the subspace's linear span, thereby creating a diverging spanned latent space. On the empirical side, we design and implement an adversarial training method, called Subspace Diverging (SD), which alleviates the robust overfitting problem and achieves state-of-the-art performance on multiple benchmarks.

References

Anish Athalye, Nicholas Carlini, and David Wagner. Obfuscated gradients give a false sense of security: Circumventing defenses to adversarial examples. In *International conference on machine learning*, pp. 274–283. PMLR, 2018. 3

Olivier Bousquet and André Elisseeff. Stability and generalization. *The Journal of Machine Learning Research*, 2:499–526, 2002. 5

Stephen P Boyd and Lieven Vandenberghe. *Convex optimization*. Cambridge university press, 2004. 24, 25

Anh Bui, Trung Le, He Zhao, Paul Montague, Olivier deVel, Tamas Abraham, and Dinh Phung. Improving adversarial robustness by enforcing local and global compactness. In *European Conference on Computer Vision*, pp. 209–223. Springer, 2020. 3, 6

Qi-Zhi Cai, Min Du, Chang Liu, and Dawn Song. Curriculum adversarial training. *arXiv preprint arXiv:1805.04807*, 2018.

N. Carlini and D. Wagner. Towards evaluating the robustness of neural networks. in 2017 ieee symposium on security and privacy (sp). *in 2017 IEEE Symposium on Security and Privacy (SP), pp.*, pp. 39–57, 2017. 1, 3

Yair Carmon, Aditi Raghunathan, Ludwig Schmidt, John C Duchi, and Percy S Liang. Unlabeled data improves adversarial robustness. *Advances in Neural Information Processing Systems*, 32, 2019.

Kwan Ho Ryan Chan, Yaodong Yu, Chong You, Haozhi Qi, John Wright, and Yi Ma. Redunet: A white-box deep network from the principle of maximizing rate reduction. *Journal of Machine Learning Research*, 23 (114):1–103, 2022. 4, 8

De Cheng, Yihong Gong, Sanping Zhou, Jinjun Wang, and Nanning Zheng. Person re-identification by multi-channel parts-based cnn with improved triplet loss function. In *Proceedings of the iEEE conference on computer vision and pattern recognition*, pp. 1335–1344, 2016a. 4

De Cheng, Yihong Gong, Sanping Zhou, Jinjun Wang, and Nanning Zheng. Person re-identification by multi-channel parts-based cnn with improved triplet loss function. *Proceedings of the IEEE conference on computer vision and pattern recognition*, pp. 1335–1344, 2016b. 4

Sumit Chopra, Raia Hadsell, and Yann LeCun. Learning a similarity metric discriminatively, with application to face verification. In *2005 IEEE Computer Society Conference on Computer Vision and Pattern Recognition (CVPR'05)*, volume 1, pp. 539–546. IEEE, 2005. 4

Rudi Cilibrasi and Paul MB Vitányi. Clustering by compression. *IEEE Transactions on Information theory*, 51(4):1523–1545, 2005.

Jeremy Cohen, Elan Rosenfeld, and Zico Kolter. Certified adversarial robustness via randomized smoothing. In *international conference on machine learning*, pp. 1310–1320. PMLR, 2019.

Francesco Croce and Matthias Hein. Reliable evaluation of adversarial robustness with an ensemble of diverse parameter-free attacks. In *International conference on machine learning*, pp. 2206–2216. PMLR, 2020. 1

Volker Fischer, Mummadi Chaithanya Kumar, Jan Hendrik Metzen, and Thomas Brox. Adversarial examples for semantic image segmentation. *arXiv preprint arXiv:1703.01101*, 2017. 1

Zhiqiang Gao, Shufei Zhang, Kaizhu Huang, Qiufeng Wang, Rui Zhang, and Chaoliang Zhong. Certifying better robust generalization for unsupervised domain adaptation. In *Proceedings of the 30th ACM International Conference on Multimedia*, pp. 2399–2410, 2022. 1

Ian J. Goodfellow, Jonathon Shlens, and Christian Szegedy. Explaining and harnessing adversarial examples. *3rd International Conference on Learning Representations,Conference Track Proceedings*, 2015. 3

Shixiang Gu and Luca Rigazio. *3rd International Conference on Learning Representations, Workshop Track Proceedings*, 2015. 1

Raia Hadsell, Sumit Chopra, and Yann LeCun. Dimensionality reduction by learning an invariant mapping. In *2006 IEEE Computer Society Conference on Computer Vision and Pattern Recognition*, volume 2, pp. 1735–1742. IEEE, 2006. 4

K. He, X. Zhang, S. Ren, and J. Sun. Deep residual learning for image recognition. In *2016 IEEE Conference on Computer Vision and Pattern Recognition (CVPR)*, 2016.

Junlin Hu, Jiwen Lu, and Yap-Peng Tan. Discriminative deep metric learning for face verification in the wild. In *Proceedings of the IEEE conference on computer vision and pattern recognition*, pp. 1875–1882, 2014. 4

Kaizhu Huang, Zenglin Xu, Rong Jin, Irwin King, and R. Michael Lyu. Robust metric learning by smooth optimization. *Proceedings of the Twenty-Sixth Conference on Uncertainty in Artificial Intelligence*, 2010. 4

Xiaojun Jia, Yong Zhang, Baoyuan Wu, Ke Ma, Jue Wang, and Xiaochun Cao. Las-at: Adversarial training with learnable attack strategy. *Conference on Computer Vision and Pattern Recognition*, 2022. 1, 3, 11, 12, 14

Gaojie Jin, Xinping Yi, Dengyu Wu, Ronghui Mu, and Xiaowei Huang. Randomized adversarial training via taylor expansion. In *Proceedings of the IEEE/CVF Conference on Computer Vision and Pattern Recognition*, pp. 16447–16457, 2023. 3, 12, 14

Harini Kannan, Alexey Kurakin, and Ian Goodfellow. Adversarial logit pairing. *arXiv preprint arXiv:1803.06373*, 2018. 1

Nupur Kumari, Mayank Singh, Abhishek Sinha, Harshitha Machiraju, Balaji Krishnamurthy, and Vineeth N Balasubramanian. Harnessing the vulnerability of latent layers in adversarially trained models. In *Proceedings of the 28th International Joint Conference on Artificial Intelligence*, pp. 2779–2785, 2019. 13

A. Kurakin, I. Goodfellow, and S Bengio. Adversarial machine learning at scale. *5th International Conference on Learning Representations, Conference Track Proceedings*, 2016. 1

Yann LeCun, Yoshua Bengio, and Geoffrey Hinton. Deep learning. *nature*, 521(7553):436–444, 2015.

Saehyung Lee, Hyungyu Lee, and Sungroh Yoon. Adversarial vertex mixup: Toward better adversarially robust generalization. In *Proceedings of the IEEE/CVF Conference on Computer Vision and Pattern Recognition*, pp. 272–281, 2020.

José Lezama, Qiang Qiu, Pablo Musé, and Guillermo Sapiro. Ole: Orthogonal low-rank embedding-a plug and play geometric loss for deep learning. In *Proceedings of the IEEE Conference on Computer Vision and Pattern Recognition*, pp. 8109–8118, 2018. 4

Binghui Li, Jikai Jin, Han Zhong, John Hopcroft, and Liwei Wang. Why robust generalization in deep learning is difficult: Perspective of expressive power. *Advances in Neural Information Processing Systems*, 35:4370–4384, 2022a. 4

Pengcheng Li, Jinfeng Yi, Bowen Zhou, and Lijun Zhang. Improving the robustness of deep neural networks via adversarial training with triplet loss. *arXiv preprint arXiv:1905.11713*, 2019. 3, 6

Tao Li, Yingwen Wu, Sizhe Chen, Kun Fang, and Xiaolin Huang. Subspace adversarial training. In *Proceedings of the IEEE/CVF Conference on Computer Vision and Pattern Recognition*, pp. 13409–13418, 2022b.

Weiyang Liu, Rongmei Lin, Zhen Liu, Lixin Liu, Zhiding Yu, Bo Dai, and Le Song. Learning towards minimum hyperspherical energy. *Advances in neural information processing systems*, 31, 2018. 3, 8

Yufei Liu, Yuan Zhou, Xin Liu, Fang Dong, Chang Wang, and Zihong Wang. Wasserstein gan-based small-sample augmentation for new-generation artificial intelligence: a case study of cancer-staging data in biology. *Engineering*, 5(1):156–163, 2019.

Chunchuan Lyu, Kaizhu Huang, and Hai-Ning Liang. A unified gradient regularization family for adversarial examples. *2015 IEEE international conference on data mining*, pp. 301–309, 2015. 1

Yi Ma, Harm Derksen, Wei Hong, and John Wright. Segmentation of multivariate mixed data via lossy data coding and compression. *IEEE transactions on pattern analysis and machine intelligence*, 29(9): 1546–1562, 2007. 24

Chengzhi Mao, Ziyuan Zhong, Junfeng Yang, Carl Vondrick, and Baishakhi Ray. Metric learning for adversarial robustness. *Advances in Neural Information Processing Systems*, 32, 2019.

Takeru Miyato, Shin-Ichi Maeda, Masanori Koyama, and Shin Ishii. Virtual adversarial training: A regularization method for supervised and semi-supervised learning. *IEEE Transactions on Pattern Analysis and Machine Intelligence*, 41(8):1979–1993, 2019. doi: 10.1109/TPAMI.2018.2858821.

Aleksander Mkadry, Aleksandar Makelov, Ludwig Schmidt, Dimitris Tsipras, and Adrian Vladu. Towards deep learning models resistant to adversarial attacks. *6th International Conference on Learning Representations*, 1050:9, 2017. 1, 11, 12, 13

Muzammal Naseer, Salman Khan, Fatih Porikli, and Fahad Shahbaz Khan. Guidance through surrogate: Toward a generic diagnostic attack. *IEEE Transactions on Neural Networks and Learning Systems*, 2022. 12, 13

Behnam Neyshabur, Srinadh Bhojanapalli, David McAllester, and Nati Srebro. Exploring generalization in deep learning. *Advances in neural information processing systems*, 30, 2017. 5

S. Nowozin, B. Cseke, and R. f-gan Tomioka. Training generative neural samplers using variational divergence minimization. in advances in neural information processing systems, pp. pp. 271–279, 2016.

D. W. Otter, J. R. Medina, and J. K. Kalita. A survey of the usages of deep learning for natural language processing. *IEEE Transactions on Neural Networks and Learning Systems*, 2020.

Tianyu Pang, Kun Xu, Yinpeng Dong, Chao Du, Ning Chen, and Jun Zhu. Rethinking softmax cross-entropy loss for adversarial robustness. *arXiv preprint arXiv:1905.10626*, 2019a.

Tianyu Pang, Kun Xu, Chao Du, Ning Chen, and Jun Zhu. Improving adversarial robustness via promoting ensemble diversity. In *International Conference on Machine Learning*, pp. 4970–4979. PMLR, 2019b.

Zhuang Qian, Shufei Zhang, Kaizhu Huang, Qiufeng Wang, Xinping Yi, Bin Gu, and Huan Xiong. Perturbation diversity certificates robust generalization. *Neural Networks*, 172:106117, 2024.

Leslie Rice, Eric Wong, and Zico Kolter. Overfitting in adversarially robust deep learning. In *International Conference on Machine Learning*, pp. 8093–8104. PMLR, 2020. 1, 2

Kevin Roth, Yannic Kilcher, and Thomas Hofmann. Adversarial training is a form of data-dependent operator norm regularization. *Advances in Neural Information Processing Systems*, 33:14973–14985, 2020.

Olivier Roy and Martin Vetterli. The effective rank: A measure of effective dimensionality. In *2007 15th European Signal Processing Conference*, pp. 606–610, 2007.

L. Schmidt, S. Santurkar, D. Tsipras, K. Talwar, and A. Madry. Adversarially robust generalization requires more data. in advances in neural information processing systems, pp. pp. 5014–5026,, 2018a.

Ludwig Schmidt, Shibani Santurkar, Dimitris Tsipras, Kunal Talwar, and Aleksander Madry. Adversarially robust generalization requires more data. *Advances in neural information processing systems*, 31, 2018b. 2, 4

Florian Schroff, Dmitry Kalenichenko, and James Philbin. Facenet: A unified embedding for face recognition and clustering. *Proceedings of the IEEE conference on computer vision and pattern recognition*, pp. 815–823, 2015. 4

Vasu Singla, Sahil Singla, Soheil Feizi, and David Jacobs. Low curvature activations reduce overfitting in adversarial training. In *Proceedings of the IEEE/CVF International Conference on Computer Vision*, pp. 16423–16433, 2021. 2

Aman Sinha, Hongseok Namkoong, Riccardo Volpi, and John Duchi. Certifying some distributional robustness with principled adversarial training. *arXiv preprint arXiv:1710.10571*, 2017.

Chawin Sitawarin, Supriyo Chakraborty, and David Wagner. Sat: Improving adversarial training via curriculum-based loss smoothing. In *Proceedings of the 14th ACM Workshop on Artificial Intelligence and Security*, pp. 25–36, 2021. 12

Chuanbiao Song, Kun He, Jiadong Lin, Liwei Wang, and John E Hopcroft. Robust local features for improving the generalization of adversarial training. *th International Conference on Learning Representations*, 2019.

Dawn Song, Kevin Eykholt, Ivan Evtimov, Earlence Fernandes, Bo Li, Amir Rahmati, Florian Tramèr, Atul Prakash, and Tadayoshi Kohno. Physical adversarial examples for object detectors. *12th USENIX Workshop on Offensive Technologies (WOOT 18)*, August 2018. 1

Ralf C Staudemeyer and Eric Rothstein Morris. Understanding lstm–a tutorial into long short-term memory recurrent neural networks. *arXiv preprint arXiv:1909.09586*, 2019.

David Stutz, Matthias Hein, and Bernt Schiele. Relating adversarially robust generalization to flat minima. In *Proceedings of the IEEE/CVF International Conference on Computer Vision*, pp. 7807–7817, 2021. 2

Jianhui Sun, Sanchit Sinha, and Aidong Zhang. Enhance diffusion to improve robust generalization. *arXiv preprint arXiv:2306.02618*, 2023. 2, 4

Yi Sun, Yuheng Chen, Xiaogang Wang, and Xiaoou Tang. Deep learning face representation by joint identification-verification. volume 27, 2014. 4

Christian Szegedy, Alexander Toshev, and Dumitru Erhan. Deep neural networks for object detection. *Advances in neural information processing systems*, 26, 2013.

Mingxing Tan, Ruoming Pang, and Quoc V Le. Efficientdet: Scalable and efficient object detection. In *Proceedings of the IEEE/CVF conference on computer vision and pattern recognition*, pp. 10781–10790, 2020.

Loring W Tu. Manifolds. In *An Introduction to Manifolds*, pp. 47–83. Springer, 2011.

Hongjun Wang and Yisen Wang. Self-ensemble adversarial training for improved robustness. *arXiv preprint arXiv:2203.09678*, 2022.

J. Wang and H. Bilateral adversarial training Zhang. Towards fast training of more robust models against adversarial attacks. *In Proceedings of the IEEE International Conference on Computer Vision*, 2019. 1, 13

Zeming Wei, Yifei Wang, Yiwen Guo, and Yisen Wang. Cfa: Class-wise calibrated fair adversarial training. In *Proceedings of the IEEE/CVF Conference on Computer Vision and Pattern Recognition*, pp. 8193–8201, 2023. 3, 4

Jon Wellner et al. *Weak convergence and empirical processes: with applications to statistics*. Springer Science & Business Media, 2013. 22

Yandong Wen, Kaipeng Zhang, Zhifeng Li, and Yu Qiao. A discriminative feature learning approach for deep face recognition. In *Computer Vision–ECCV 2016: 14th European Conference, Amsterdam, The Netherlands, October 11–14, 2016, Proceedings, Part VII 14*, pp. 499–515. Springer, 2016. 4

Dongxian Wu, Shu-Tao Xia, and Yisen Wang. Adversarial weight perturbation helps robust generalization. *Advances in Neural Information Processing Systems*, 33:2958–2969, 2020. 1, 3, 11, 12, 14

Huan Xu and Shie Mannor. Robustness and generalization. *The 23rd Conference on Learning Theory*, 86 (3):391–423, 2012. 5, 9

Yao-Yuan Yang, Cyrus Rashtchian, Hongyang Zhang, Russ R Salakhutdinov, and Kamalika Chaudhuri. A closer look at accuracy vs. robustness. *Advances in neural information processing systems*, 33:8588–8601, 2020.

Mingyang Yi, Lu Hou, Jiacheng Sun, Lifeng Shang, Xin Jiang, Qun Liu, and Zhiming Ma. Improved ood generalization via adversarial training and pretraing. In *International Conference on Machine Learning*, pp. 11987–11997. PMLR, 2021.

D. Yin, R. Kannan, and P. Bartlett. Rademacher complexity for adversarially robust generalization. in international conference on machine learning, pp. pp. 7085–7094, 2019. 4

Saeideh Yousefzadeh, Hamidreza Pourreza, and Hamidreza Mahyar. A triplet-loss dilated residual network for high-resolution representation learning in image retrieval. *Journal of Signal Processing Systems*, pp. 1–13, 2023. 4

Yaodong Yu, Kwan Ho Ryan Chan, Chong You, Chaobing Song, and Yi Ma. Learning diverse and discriminative representations via the principle of maximal coding rate reduction. *Advances in Neural Information Processing Systems*, 33:9422–9434, 2020. 4, 8, 24

Sergey Zagoruyko and Nikos Komodakis. Wide residual networks. *CoRR*, abs/1605.07146, 2016. URL http://arxiv.org/abs/1605.07146.

Runtian Zhai, Tianle Cai, Di He, Chen Dan, Kun He, John Hopcroft, and Liwei Wang. Adversarially robust generalization just requires more unlabeled data. *Advances in Neural Information Processing Systems*, 2019.

Haichao Zhang and Jianyu Wang. Defense against adversarial attacks using feature scattering-based adversarial training. *Advances in Neural Information Processing Systems*, 32, 2019. 1, 2, 3, 11, 12, 13

Hongyang Zhang, Yaodong Yu, Jiantao Jiao, Eric Xing, Laurent El Ghaoui, and Michael Jordan. Theoretically principled trade-off between robustness and accuracy. pp. 7472–7482. PMLR, 2019. 1, 4, 11

Jingfeng Zhang, Xilie Xu, Bo Han, Gang Niu, Lizhen Cui, Masashi Sugiyama, and Mohan Kankanhalli. Attacks which do not kill training make adversarial learning stronger. In *International conference on machine learning*, pp. 11278–11287. PMLR, 2020a. 3

Jingfeng Zhang, Xilie Xu, Bo Han, Gang Niu, Lizhen Cui, Masashi Sugiyama, and Mohan Kankanhalli. Attacks which do not kill training make adversarial learning stronger. In *International conference on machine learning*, pp. 11278–11287. PMLR, 2020b. 12

Jingfeng Zhang, Jianing Zhu, Gang Niu, Bo Han, Masashi Sugiyama, and Mohan Kankanhalli. Geometry-aware instance-reweighted adversarial training. *arXiv preprint arXiv:2010.01736*, 2020c. 3, 12

Shufei Zhang, Kaizhu Huang, Jianke Zhu, and Yang Liu. Manifold adversarial learning. *Neural Networks*, 2018.

Shufei Zhang, Zhuang Qian, Kaizhu Huang, Qiufeng Wang, Rui Zhang, and Xinping Yi. Towards better robust generalization with shift consistency regularization. *International Conference on Machine Learning*, pp. 12524–12534, 2021. 2, 3, 4, 5, 6, 9, 12, 13, 14, 23

Shufei Zhang, Zhuang Qian, Kaizhu Huang, Qiu-Feng Wang, Bin Gu, Huan Xiong, and Xinping Yi. Inter-feature relationship certifies robust generalization of adversarial training. *International Journal of Computer Vision*, pp. 1–17, 2024. 24

Long Zhao, Ting Liu, Xi Peng, and Dimitris Metaxas. Maximum-entropy adversarial data augmentation for improved generalization and robustness. *Advances in Neural Information Processing Systems*, 33: 14435–14447, 2020.

Zhong-Qiu Zhao, Peng Zheng, Shou-Tao Xu, and Xindong Wu. Object detection with deep learning: A review. *IEEE Transactions on Neural Networks and Learning Systems*, 30(11):3212–3232, 2019. doi: 10.1109/TNNLS.2018.2876865.

A Theory Proof

Proof of Theorem 3.1

Theorem 3.1 *Given the clean data matrix $\boldsymbol{X}_i$ and adversarial data matrix $\boldsymbol{X}_i^{adv}$ that both contain N_i samples of i-th class over the training set, the sets of clean data C_i and adversarial data C_i^{adv} of i-th class over the underlying data distribution, and the DNN f_θ that maps data samples to latent features with dimension r, if the loss function $l(\cdot)$ of $f_\theta(\cdot)$ is t Lipschitz and constant values L_d and L_u exist, then for any $\delta > 0$, with the probability at least $1-\delta$, we have*

$$\begin{aligned}
&\varepsilon_{RGE} \leq \varepsilon_{GE} + \frac{tU^2 L_d}{N}||\nabla \boldsymbol{T}_d||_2 + \frac{tV^2 L_u}{K}||\nabla \boldsymbol{T}||_2 + \sqrt{\frac{2K\ln 2 + 2\ln\left(\frac{1}{\sigma}\right)}{N}},\\
&\textit{where} \quad \nabla \boldsymbol{T}_d = \boldsymbol{T}_d^{adv} - \boldsymbol{T}_d, \qquad \nabla \boldsymbol{T} = \boldsymbol{T}^{adv} - \boldsymbol{T},\\
&\qquad\qquad U = \frac{1}{N}\sum_{n=1}^{N}||f_\theta(x_n)||_2, \quad V = \frac{1}{K}\sum_{i=1}^{K}||\mathbb{E}\left[f_\theta(x) \mid x \in C_i\right]||_2,
\end{aligned}$$

M is the upper bound of the loss over the whole underlying data manifold. $\bigtriangledown \boldsymbol{T}_d$ and $\bigtriangledown \boldsymbol{T}$ denote the Gram matrix difference over the training set and the underlying data distribution respectively,

$$\begin{aligned}
\bigtriangledown \boldsymbol{T}_d &= \begin{bmatrix} \left(\boldsymbol{Z}_1^{adv}\right)^\top \boldsymbol{Z}_1^{adv} - \left(\boldsymbol{Z}_1\right)^\top \boldsymbol{Z}_1, & \cdots, & \left(\boldsymbol{Z}_1^{adv}\right)^\top \boldsymbol{Z}_K^{adv} - \left(\boldsymbol{Z}_1\right)^\top \boldsymbol{Z}_K \\ \ddots & \ddots & \ddots \\ \left(\boldsymbol{Z}_K^{adv}\right)^\top \boldsymbol{Z}_1^{adv} - \left(\boldsymbol{Z}_K\right)^\top \boldsymbol{Z}_1, & \cdots, & \left(\boldsymbol{Z}_K^{adv}\right)^\top \boldsymbol{Z}_K^{adv} - \left(\boldsymbol{Z}_K\right)^\top \boldsymbol{Z}_K \end{bmatrix},\\
\bigtriangledown \boldsymbol{T} &= \begin{bmatrix} \left(z_1^{adv}\right)^\top z_1^{adv} - \left(z_1\right)^\top z_1, & \cdots, & \left(z_1^{adv}\right)^\top z_K^{adv} - \left(z_1\right)^\top z_K \\ \ddots & \ddots & \ddots \\ \left(z_K^{adv}\right)^\top z_1^{adv} - \left(z_K\right)^\top z_1, & \cdots, & \left(z_K^{adv}\right)^\top z_K^{adv} - \left(z_K\right)^\top z_K \end{bmatrix},
\end{aligned} \tag{12}$$

$$\begin{aligned}
&\textit{where} \quad \boldsymbol{Z}_i = \frac{f_\theta\left(\boldsymbol{X}_i\right)}{\|f_\theta\left(\boldsymbol{X}_i\right)\|_{2,col}}, \quad \boldsymbol{Z}_i^{adv} = \frac{f_\theta\left(\boldsymbol{X}_i^{adv}\right)}{\|f_\theta\left(\boldsymbol{X}_i^{adv}\right)\|_{2,col}}, \quad \boldsymbol{Z}_i, \boldsymbol{Z}_i^{adv} \in \mathbb{R}^{r\times N_i},\\
&z_i = \frac{\mathbb{E}\left[f_\theta\left(x\right) \mid x \in C_i\right]}{\|\mathbb{E}\left[f_\theta\left(x\right) \mid x \in C_i\right]\|_2}, \quad z_i^{adv} = \frac{\mathbb{E}\left[f_\theta\left(x^{adv}\right) \mid x^{adv} \in C_i^{adv}\right]}{\|\mathbb{E}\left[f_\theta\left(x^{adv}\right) \mid x \in C_i^{adv}\right]\|_2}, \quad z_i, z_i^{adv} \in \mathbb{R}^r.
\end{aligned}$$

$\|\cdot\|_{2,col}$ *represents the calculation of the Euclidean norm of column vectors in the matrix.*

proof : Let $\{N_1, N_2, N_3, \ldots, N_K\}$ be a multinomial random variable set, where $\{N_i\}_{i=1}^K \in [0, N]$. N and K denote the total number of training samples and the total number of classes respectively. With the probability distribution set for the underlying classes $\{\mu(C_1), \mu(C_2), \ldots, \mu(C_i), \ldots \mu(C_K)\}$, following Breteganolle-Huber-Carel inequality (Proposition A6.6 of (Wellner et al., 2013)):

$$Pr\{\sum_{i=K}^{K}|\frac{N_i}{N} - \mu(C_i)| \geq \lambda\} \leq 2^K exp(\frac{-2N\lambda^2}{2}).$$

With the probability at least $1-\delta$, we can get:

$$\sum_{i=1}^{K}\left|\frac{N_i}{N} - \mu\left(C_i\right)\right| \leq \sqrt{\frac{2K\ln 2 + 2\ln\left(\frac{1}{\sigma}\right)}{N}}.$$

$$\varepsilon_{RGE} = \left|\mathbb{E}\left[l\left(f_\theta(x^{adv}), y\right) \mid x \in X\right] - \frac{1}{N}\sum_{n=1}^{N} l\left(f_\theta(x_n^{adv}), y_n\right)\right|$$

$$
\begin{aligned}
&= \left| \sum_{i=1}^{K} \mathbb{E}\left[l\left(f_\theta(x^{adv}), y\right) \mid x \in C_i \right] \mu(C_i) - \frac{1}{N} \sum_{n=1}^{N} l\left(f_\theta(x_n^{adv}), y_n\right) \right| \\
&= \Bigg| \sum_{i=1}^{K} \left[\mathbb{E}\left[l\left(f_\theta(x^{adv}), y\right) \mid x \in C_i \right] + \mathbb{E}\left[l\left(f_\theta(x), y\right) \mid x \in C_i \right] - \mathbb{E}\left[l\left(f_\theta(x), y\right) \mid x \in C_i \right] \right] \mu(C_i) - \\
&\quad \frac{1}{N} \sum_{n=1}^{N} \left[l\left(f_\theta(x_n^{adv}), y_n\right) - l\left(f_\theta(x_n), y_n\right) + l\left(f_\theta(x_n), y_n\right) \right] \Bigg| \\
&\leq \left| \sum_{i=1}^{K} \mathbb{E}\left[l\left(f_\theta(x), y\right) \mid x \in C_i \right] \mu(C_i) - \frac{1}{N} \sum_{n=1}^{N} l\left(f_\theta(x_n), y_n\right) \right| + \left| \sum_{i=1}^{K} \left[\mathbb{E}\left[l\left(f_\theta(x^{adv}), y\right) \mid x \in C_i \right] - \right. \right. \\
&\left. \left. \mathbb{E}\left[l\left(f_\theta(x), y\right) \mid x \in C_i \right] \mu(C_i) - \frac{1}{N} \sum_{n=1}^{N} \left[l\left(f_\theta(x_n^{adv}), y_n\right) - l\left(f_\theta(x_n), y_n\right) \right] \right| .
\end{aligned}
$$

Denoting $e = \frac{N}{K}$, we can further reformat the above as

$$
\begin{aligned}
&= \varepsilon_{GE} + \Bigg| \sum_{i=1}^{K} \left[\mathbb{E}\left[l\left(f_\theta(x^{adv}), y\right) \mid x \in C_i \right] - \mathbb{E}\left[l\left(f_\theta(x), y\right) \mid x \in C_i \right] \right] \mu(C_i) - \frac{1}{N} \sum_{n=1}^{N} \left[l\left(f_\theta(x_n^{adv}), y_n\right) - l\left(f_\theta(x_n), y_n\right) \right] \\
&\quad + \sum_{i=1}^{K} \left[\mathbb{E}\left[l\left(f_\theta(x^{adv}), y\right) \mid x \in C_i \right] - \mathbb{E}\left[l\left(f_\theta(x), y\right) \mid x \in C_i \right] \right] \frac{e}{N} - \sum_{i=1}^{K} \left[\mathbb{E}\left[l\left(f_\theta(x), y\right) \mid x \in C_i \right] - \mathbb{E}\left[l\left(f_\theta(x), y\right) \mid x \in C_i \right] \right] \frac{e}{N} \Bigg| \\
&\leq \varepsilon_{GE} + \Bigg| \sum_{i=1}^{K} \left[\mathbb{E}\left[l\left(f_\theta(x^{adv}), y\right) \mid x \in C_i \right] - \mathbb{E}\left[l\left(f_\theta(x), y\right) \mid x \in C_i \right] \right] \mu(C_i) - \sum_{i=1}^{K} \left[\mathbb{E}\left[l\left(f_\theta(x^{adv}), y\right) \mid x \in C_i \right] - \right. \\
&\left. \mathbb{E}\left[l\left(f_\theta(x), y\right) \mid x \in C_i \right] \frac{e}{N} \right| + \left| \frac{1}{N} \sum_{n=1}^{N} \left[l\left(f_\theta(x_n^{adv}), y_n\right) - l\left(f_\theta(x_n), y_n\right) \right] - \frac{e}{N} \sum_{i=1}^{K} \left[\mathbb{E}\left[l\left(f_\theta(x^{adv}), y\right) - l\left(f_\theta(x), y\right) \mid x \in C_i \right] \right] \right| \\
&\leq \varepsilon_{GE} + \left| \sum_{i=1}^{K} \mathbb{E}\left[l\left(f_\theta(x^{adv}), y\right) - l\left(f_\theta(x), y\right) \mid x \in C_i \right] \frac{e}{N} - \frac{1}{N} \sum_{n=1}^{N} \left[l\left(f_\theta(x_n^{adv}), y_n\right) - l\left(f_\theta(x_n), y_n\right) \right] \right| \\
&\quad + M * \left| \sum_{i=1}^{K} (\mu(C_i) - \frac{e}{N}) \right| .
\end{aligned}
$$

Based on Breteganolle-Huber-Carel inequality and a widely used assumption that $|l\left(f_\theta(x_1), y_1\right) - l\left(f_\theta(x_2), y_2\right)| \leq t||f_\theta(x_1) - f_\theta(x_2)||_2^2$ from (Zhang et al., 2021), we get:

$$
\begin{aligned}
&\leq \varepsilon_{GE} + \left| \sum_{i=1}^{K} \mathbb{E}\left[l\left(f_\theta(x^{adv}), y\right) - l\left(f_\theta(x), y\right) \mid x \in C_i \right] \frac{e}{N} - \frac{1}{N} \sum_{n=1}^{N} \left[l\left(f_\theta(x_n^{adv}), y_n\right) - l\left(f_\theta(x_n), y_n\right) \right] \right| + \\
&\quad + \sqrt{\frac{2K \ln 2 + 2 \ln\left(\frac{1}{\sigma}\right)}{N}} \\
&\leq \varepsilon_{GE} + \frac{t}{N} * \left| \sum_{n=1}^{N} \left[||f_\theta(x_n^{adv}) - f_\theta(x_n)||_2^2 \right] - e \sum_{i=1}^{K} \mathbb{E}\left[||(f_\theta(x^{adv}) - f_\theta(x))||_2^2 \mid x \in C_i \right] \right| + \sqrt{\frac{2K \ln 2 + 2 \ln\left(\frac{1}{\sigma}\right)}{N}} \\
&\leq \varepsilon_{GE} + \frac{t}{N} * \left| \sum_{j=1}^{N} \left[||f_\theta(x_n^{adv}) - f_\theta(x_n)||_2^2 \right] + e \sum_{i=1}^{K} \mathbb{E}\left[||(f_\theta(x^{adv}) - f_\theta(x))||_2^2 \mid x \in C_i \right] \right| + \sqrt{\frac{2K \ln 2 + 2 \ln\left(\frac{1}{\sigma}\right)}{N}}
\end{aligned}
$$

$$= \varepsilon_{GE} + \frac{t}{N} * \left| \sum_{n=1}^{N} \left[||f_\theta(x_n^{adv}) - f_\theta(x_n)||_2^2 \right] + \sum_{i=1}^{K} \mathbb{E}\left[||(f_\theta(x^{adv}) - f_\theta(x))||_2^2 \frac{N}{K} \mid x \in C_i \right] \right| + \sqrt{\frac{2K\ln 2 + 2\ln\left(\frac{1}{\sigma}\right)}{N}}.$$

Let $f_\theta(\boldsymbol{X}_d) \in \mathbb{R}^{r\times N}$ and $f_\theta(\boldsymbol{X}_u) \in \mathbb{R}^{r\times K}$ represent the training and expected underlying feature matrix, respectively, where $f_\theta(\boldsymbol{X}_u) = [\mathbb{E}[f(x)] \mid x \in C_i]_{i=1}^{K}$. Additionally, let $f_\theta\left(\boldsymbol{X}_d^{adv}\right) \in \mathbb{R}^{r\times N}$ and $f_\theta\left(\boldsymbol{X}_u^{adv}\right) \in \mathbb{R}^{r\times K}$ denote the corresponding adversarial feature sets. We can gain that

$$= \varepsilon_{GE} + \frac{t}{N} \left| ||f_\theta\left(\boldsymbol{X}_d^{adv}\right) - f_\theta\left(\boldsymbol{X}_d\right)||_2^2 + ||\mathbb{E}\left[f_\theta(\boldsymbol{X}_u^{adv})\right] - \mathbb{E}\left[f_\theta(\boldsymbol{X}_u)\right]||_2^2 \frac{N}{K} \right| + \sqrt{\frac{2K\ln 2 + 2\ln\left(\frac{1}{\sigma}\right)}{N}}.$$

If we borrow the theory from (Zhang et al., 2024), since $[f_\theta(X)]^2$ is a smooth function and with Lagrange mean value theorem, there exist ratio constants L_t and L_u, satisfying $L_d||\left[f_\theta(\boldsymbol{X}_D^{adv})\right]^2 - [f_\theta(\boldsymbol{X}_D)]^2||_2 \geq ||f_\theta(\boldsymbol{X}_D^{adv}) - f_\theta(\boldsymbol{X}_D)||_2^2$ and $L_u||\mathbb{E}\left[f_\theta(\boldsymbol{X}_u^{adv})\right]^2 - \mathbb{E}\left[f_\theta(\boldsymbol{X}_u)\right]^2||_2 \geq ||\mathbb{E}\left[f_\theta(\boldsymbol{X}_u^{adv})\right] - \mathbb{E}\left[f_\theta(\boldsymbol{X}_u)\right]||_2^2$. We can get

$$\begin{aligned}
\varepsilon_{RGE} &\leq \varepsilon_{GE} + \frac{t}{N} \left| L_d||\left[f_\theta(\boldsymbol{X}_D^{adv})\right]^2 - [f_\theta(\boldsymbol{X}_D)]^2||_2 + L_u||\mathbb{E}\left[f_\theta(\boldsymbol{X}_u^{adv})\right]^2 - \mathbb{E}\left[f_\theta(\boldsymbol{X}_u)\right]^2||_2 \frac{N}{K} \right| + \\
&\sqrt{\frac{2K\ln 2 + 2\ln\left(\frac{1}{\sigma}\right)}{N}} \\
&= \varepsilon_{GE} + \left| \frac{tU^2 L_d}{N}||\left(\boldsymbol{T}_d^{adv} - \boldsymbol{T}_d\right)||_2 + \frac{tV^2 L_u}{N}||\left(\boldsymbol{T}^{adv} - \boldsymbol{T}\right)||_2 \frac{N}{K} \right| + \sqrt{\frac{2K\ln 2 + 2\ln\left(\frac{1}{\sigma}\right)}{N}} \\
&= \varepsilon_{GE} + \frac{tU^2 L_d}{N}||\nabla \boldsymbol{T}_d||_2 + \frac{tV^2 L_u}{K}||\nabla \boldsymbol{T}||_2 + \sqrt{\frac{2K\ln 2 + 2\ln\left(\frac{1}{\sigma}\right)}{N}}.
\end{aligned}$$

Proof of Theorem 3.2

Theorem 3.2 *Let the latent space span $\boldsymbol{S}$ be a non-singular matrix that covers all subspans and is denoted as $\{S_i\}_{i=1}^{K} \in S$, and $\boldsymbol{I}$ be the identity matrix. For any vectors $\gamma_i, \gamma_j \in S_i$, S_j, where $\forall i, j \leq K$, and $i \neq j$, and vectors $\gamma_{iu}, \gamma_{iv} \in S_i$, the implication relationship is:*

$$\begin{aligned}
\max \mathrm{Vol}(\boldsymbol{S}) &\Longrightarrow \min \langle \gamma_i, \gamma_j \rangle, \\
\min \mathrm{Vol}(\boldsymbol{I} + \boldsymbol{S}_i) &\Longrightarrow \max \langle \gamma_{iu}, \gamma_{iv} \rangle.
\end{aligned} \tag{13}$$

To establish the proof, we initially introduce the $\log\det(\cdot)$ function, leveraging its concavity as detailed in (Boyd & Vandenberghe, 2004). Prior research (Yu et al., 2020) has demonstrated that maximizing $\log\det(\boldsymbol{S})$ is equal to maximize $\log\det(\boldsymbol{I} + \boldsymbol{S})$, and Ma et al. (2007) has further illustrated that $\log\det(\boldsymbol{I} + \boldsymbol{S}) \approx \log\det(\boldsymbol{I} + \hat{\boldsymbol{Z}}^\top \hat{\boldsymbol{Z}})$ for feature representation, where $\hat{\boldsymbol{Z}} = f(\boldsymbol{X})$. Consequently, this allows:

$$\max_{\boldsymbol{Z}} \ \log\det(\boldsymbol{S}) \Longleftrightarrow \max_{\boldsymbol{Z}} \ \log\det(\boldsymbol{I} + \boldsymbol{Z}^\top \boldsymbol{Z}), \tag{14}$$

where $\boldsymbol{Z}$ is the normalized feature matrix of $\hat{\boldsymbol{Z}}$. When $\forall i, j \leq n, i \neq j$ and $\forall\ \gamma_i, \gamma_j \in \boldsymbol{S}_i$, $\boldsymbol{S}_j$ respectively, $\langle \gamma_i, \gamma_j \rangle = 0$, the latent spanned space can be denoted as $\boldsymbol{S}^*$, and their feature representation can be defined as $\boldsymbol{Z}^*$. In addition, we define the matrix $\boldsymbol{D}$ as:

$$\boldsymbol{D} = \boldsymbol{I} + \boldsymbol{Z}^\top \boldsymbol{Z}. \tag{15}$$

We assume that $\boldsymbol{D}$ is a non-singular matrix and denote $\boldsymbol{D}^\top$ as the transpose matrix of $\boldsymbol{D}$. Because the strict concavity of $\log\det(\cdot)$, we can get the relationship as follow:

$$\log\det(\boldsymbol{D}) - \log\det(\boldsymbol{D}^*) \leq < \nabla \log\det(\boldsymbol{D}^*), \boldsymbol{D} - \boldsymbol{D}^* > . \tag{16}$$

From (Boyd & Vandenberghe, 2004), we can get that $\nabla \log\det(\boldsymbol{D}^*) = \boldsymbol{D}^{*-1}$. In addition, due to $\boldsymbol{D}^{*-1} = (\boldsymbol{D}^{*-1})^\top$, the RHS of Equation 16 can be shown as:

$$
\begin{aligned}
&=< \left(\boldsymbol{D}^{*-1}\right), (\boldsymbol{D} - \boldsymbol{D}^*) > \\
&=< \left(\boldsymbol{D}^{*-1}\right), \boldsymbol{D} > - < \left(\boldsymbol{D}^{*-1}\right), \boldsymbol{D}^* >
\end{aligned}
$$

We set the matrix $\left(\boldsymbol{D}^{*-1}\right)\boldsymbol{D}$ as $\boldsymbol{G}$

$$
\begin{aligned}
&= \mathrm{tr}(\boldsymbol{G}) - \mathrm{tr}(\boldsymbol{I}) \\
&= N - N \\
&= 0.
\end{aligned}
$$

The matrix $\boldsymbol{G}$ can be represented as follows:

$$
\boldsymbol{G} = \begin{bmatrix} 1 & \cdots & \emptyset \\ \vdots & \ddots & \vdots \\ \emptyset & \cdots & 1 \end{bmatrix}, \tag{17}
$$

where $\emptyset$ are the irrelevant numbers with the process of calculating trace. Thus, when the volume of the latent span reaches its maximum value, each subspace is independent of each other and its matrix $\boldsymbol{D}$ is a non-singular matrix. We can gain the implication relationship as:

$$
\max \mathrm{Vol}(\boldsymbol{S}) \Longrightarrow \min \langle \gamma_i, \gamma_j \rangle . \tag{18}
$$

The same theory as above, the relationship is also satisfied:

$$
\min_{\boldsymbol{Z}_i} \ \log\det(\boldsymbol{I} + \boldsymbol{S}_i) \Longleftrightarrow \min_{\boldsymbol{Z}_i} \log\det(\boldsymbol{I} + {\boldsymbol{Z}_i}^\top \boldsymbol{Z}_i), \tag{19}
$$

where $\boldsymbol{Z}_i \in \mathbb{R}^{r \times T}$ is i-th class feature matrix,which includes T samples, and $\boldsymbol{Z}_i = [z_{i_t}]_{t=1}^{\mathrm{T}}$. The matrix $\boldsymbol{I} + \boldsymbol{Z}_i^\top \boldsymbol{Z}_i$ can be defined as matrix $\boldsymbol{Q}_i$:

$$
\boldsymbol{Q}_i = \boldsymbol{I} + \begin{bmatrix} < z_{i_1}, z_{i_1} > & \cdots & < z_{i_1}, z_{i_\mathrm{T}} > \\ \vdots & \ddots & \vdots \\ < z_{i_\mathrm{T}}, z_{i_1} > & \cdots & < z_{i_\mathrm{T}}, z_{i_\mathrm{T}} > \end{bmatrix}. \tag{20}
$$

For $\forall a, b \in \boldsymbol{Z}_i$, and $\langle a, b \rangle = 1$, $\det(\boldsymbol{Z}i^\top \boldsymbol{Z}i)$ will be close to attaining the minimum value of 0. Correspondingly, $\forall \gamma_{iu}, \gamma_{iv} \in \boldsymbol{S}_i$, there will also appear $\langle \gamma_i, \gamma_j \rangle = |\gamma_i| \times |\gamma_j|$. Since $\log\det(\boldsymbol{Z}_i^\top \boldsymbol{Z}_i)$ and $\log\det(\boldsymbol{Q}_i)$ share the same trends, $\log\det(\boldsymbol{Q}_i)$ will also reach its minimization value.

Therefore, we gain the implication that

$$
\min \mathrm{Vol}(\boldsymbol{I} + \boldsymbol{S}_i) \Longrightarrow \max \langle \gamma_{iu}, \gamma_{iv} \rangle . \tag{21}
$$

Our proof has been completed.